TIME DELAY COSMOGRAPHY

For a review: https://link.springer.com/article/10.1007/s00159-022-00145-y
See also: https://arxiv.org/pdf/2505.22738

MULTIPLE IMAGES FROM STRONG LENSING

Multiply imaged time-variable sources can be used to measure absolute distances as a function of redshifts and thus determine cosmological parameters, chiefly the Hubble Constant H_0.

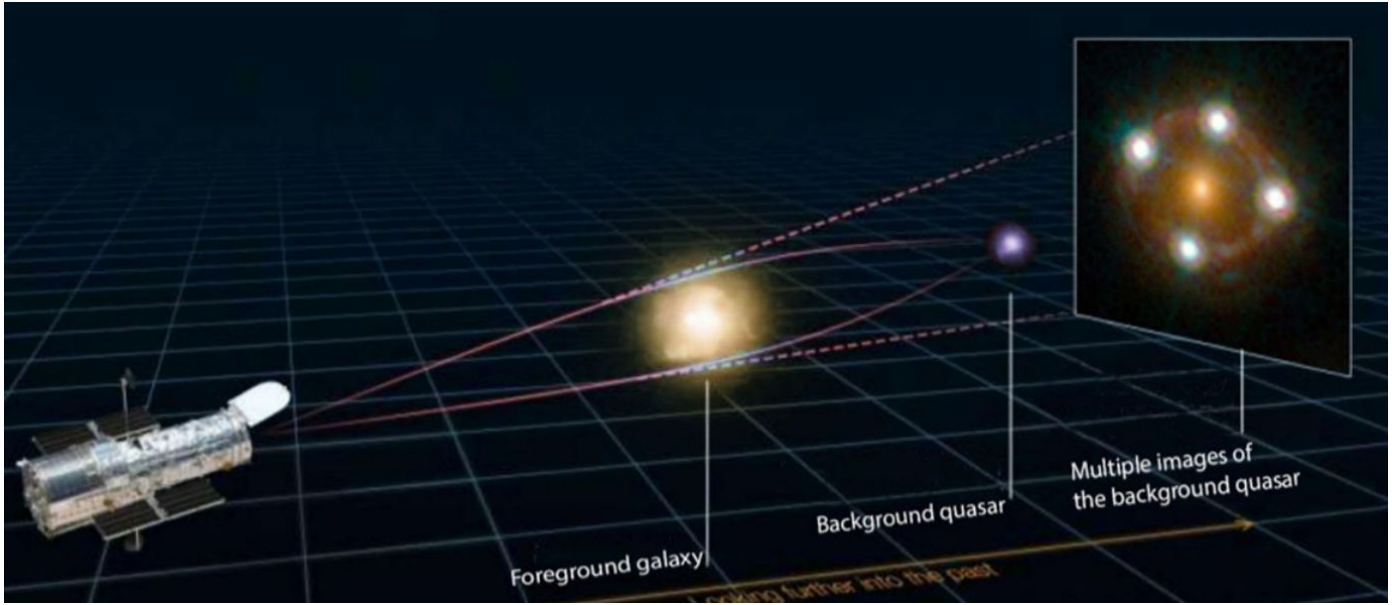

When a distant variable source (e.g., a supernova or a quasar) is multiply imaged by a foreground mass distribution (e.g. a galaxy or cluster of galaxies), the multiple images appear offset in time to the observer. The delay(s) between the leading image and trailing one(s) arise from the combination of two effects. The first one is the difference in length of the optical paths. The second is a general relativistic effect, called the Shapiro (1964) delay, owing to the difference in gravitational potential experienced by the photons along the paths.

TIME DELAY COSMOGRAPHY

The time delay between image A and image B is given by:

$$\Delta\tau_{\mathrm{AB}} = \frac{D_{\Delta \mathrm{t}}}{c}\Delta\Phi_{\mathrm{AB}}$$

$$D_{\Delta \mathrm{t}} \equiv (1+z_{\mathrm{d}})\frac{D_{\mathrm{d}}D_{\mathrm{s}}}{D_{\mathrm{ds}}}$$

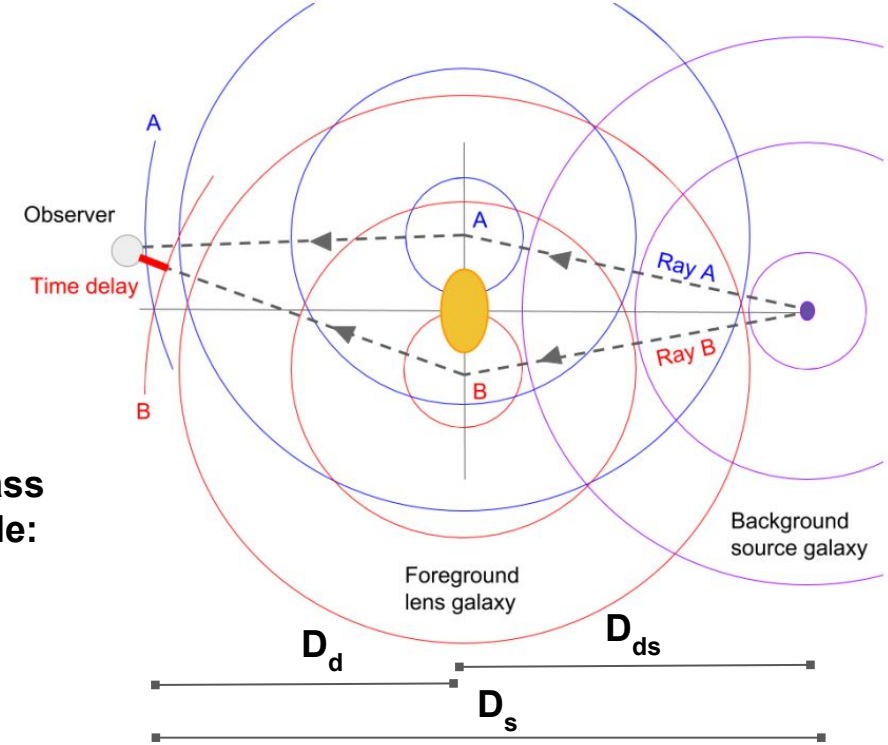

$\Delta\,\phi$: Fermat potential difference between two image position. It can be predicted given a model for the mass distribution of the lens, along with the deflection angle:

$$\phi = \frac{1}{2}(\theta-\beta)^2 - \psi(\theta)$$

Geometrical delay

Lens potential
(Shapiro delay)

TIME DELAY COSMOGRAPHY

Steps:

- **Measure the time-delay between two images**
  - **The basic idea is to detect variations in the brightness of the quasar images in a lens system and use these variations to determine the time delay between the multiple images, given that the intrinsic brightness variations of the quasar manifest in each of the multiple images.**
- **Measure and model the potential**
- **Infer the time delay distance $D_{\Delta t}$**
- **Convert it into cosmological parameters**

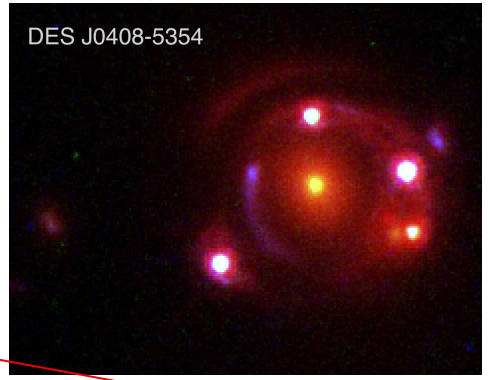

H_0 measurements of 6 lensed quasars from the H0LiCOW program

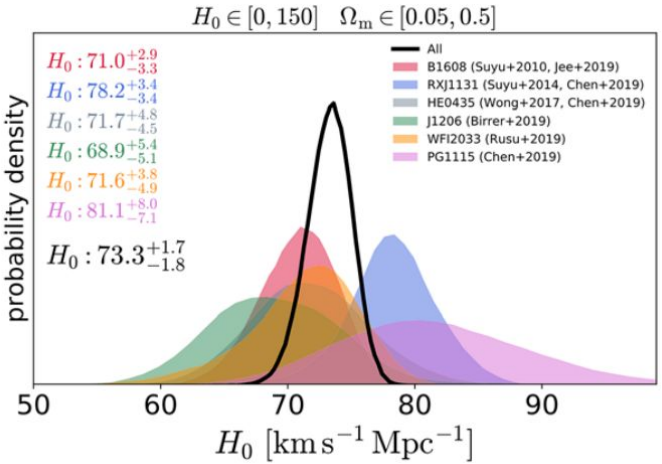

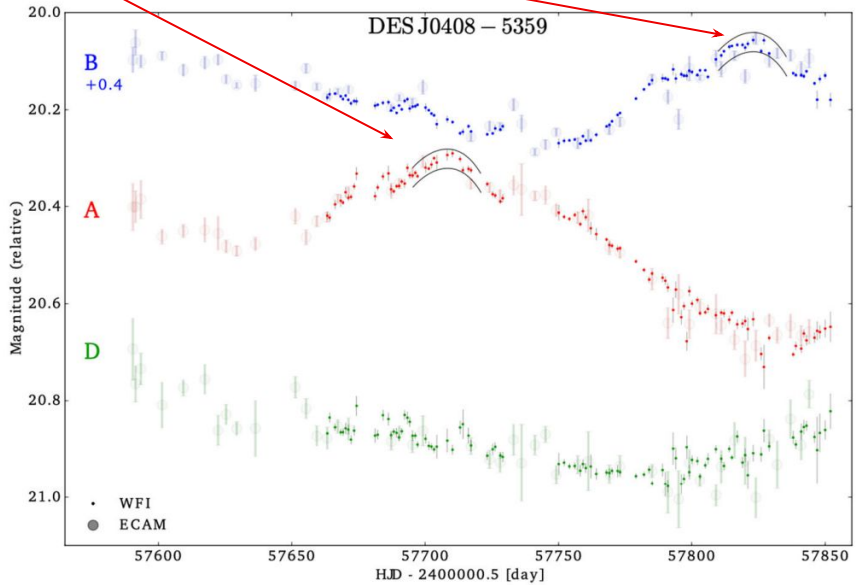

TIME DELAY COSMOGRAPHY

Multiply-imaged supernovae provide a novel means of constraining H_0.

Such measurements require a combination of precise models of the lensing mass distribution and an accurate estimate of the relative time delays between arrival of the multiple images.

Only three multiply-imaged SNe found so far: Refsdal, H0pe, SN Encore

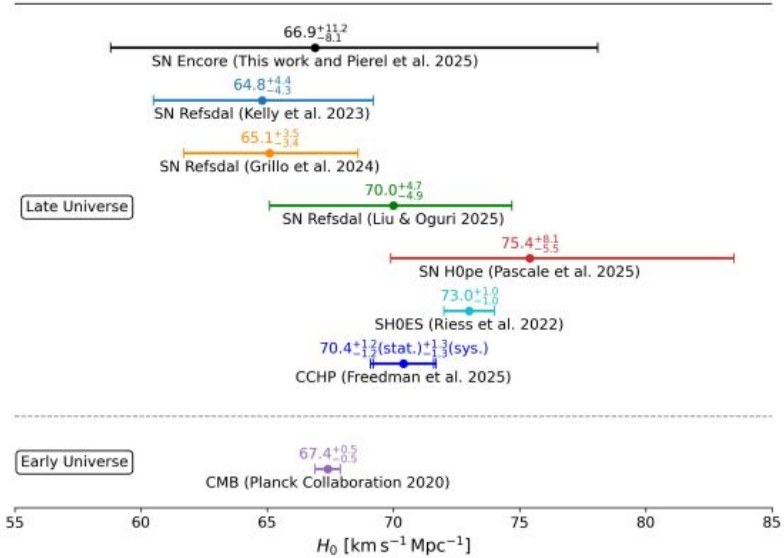

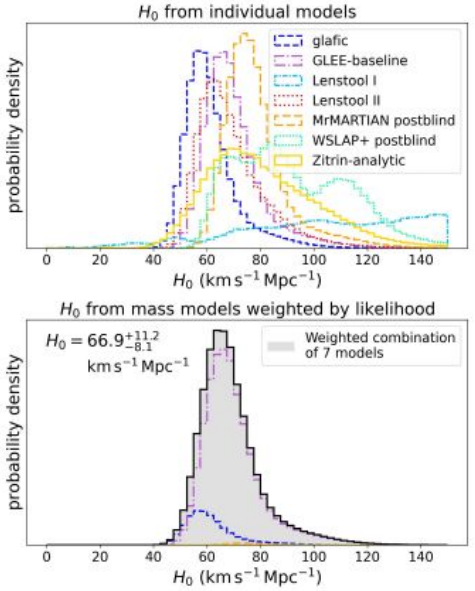

Fig. 8: H_0 inference from SN Encore using the time-delay measurement $\Delta t_{1b,1a}$ by Pierel et al. (2026). Top: Inferred H_0 distribution from the mass models of the seven modeling teams via blind analysis, where the mass models and the time delay were kept blind to each other throughout and combined after unblinding without modifications. Bottom: H_0 from the combined mass model, weighted by each model's likelihood. The weights were determined before unblinding (see Table 2). Our $H_0 = 66.9^{+11.2}_{-8.1}$ km s^{-1} Mpc^{-1} has most of its uncertainty stemming from the current time-delay measurement, which will be significantly reduced thanks to approved HST and JWST observations of this unique lens system.

See also Grillo+24

Cosmology with supernova Encore in the strong lensing cluster MACS J0138−2155 (Pierel+25, Suyu+25)

TIME DELAY COSMOGRAPHY

Remarkably, a sibling to SN Encore (SN “Requiem”) was discovered in the same host galaxy, making the MACS J0138.0-2155 cluster the first system known to produce more than one observed multiply-imaged SN. SN Requiem has a fourth image that is expected to appear within a few years, providing an unprecedented decade-long baseline for time-delay cosmography. The fourth image of SN Requiem is expected to appear:

For H_0 =73 km/s/Mpc in late 2026
For H_0 =67 km/s/Mpc mid 2027

The long time delays of the next-appearing SN Requiem and SN Encore images provide excellent opportunities to measure H0 with 2-3% uncertainty

Cosmology with supernova Encore (z=1.95) in the strong lensing cluster MACS J0138−2155 (Pierel+25, Suyu+25)

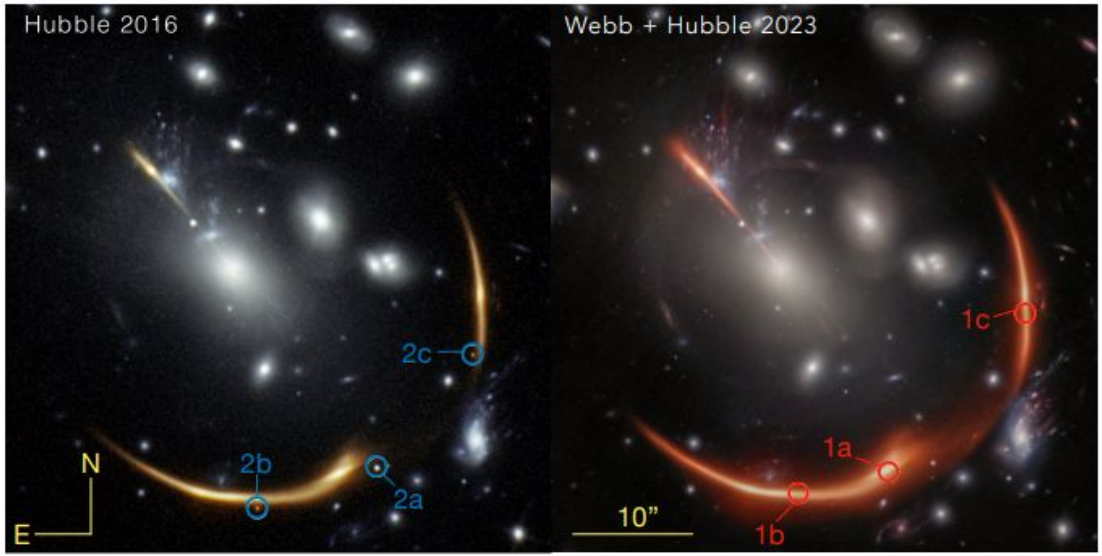

Figure 1. *Left*: *HST* WFC3/IR two-color image in the region of MACS J0138.0−2155 from 2016, using F105W (blue) and F160W (orange). SN Requiem is marked in its three visible image positions by blue circles, notably absent in 2023. *Right:* Combined *JWST*/NIRCam and *HST*/WFC3 color image from programs 6549 and 16264 (Table 1). The filters used are F105W+F115W+F125W (blue), F150W+F160W+F200W (green), and F277W+F356W+F444W (red). The images were drizzled to $0\farcs02$/pix, and the image scale and orientation are as shown. The three detected image positions of SN Encore are circled in red, but it is not visible at this scale (See Figure 4 for a zoom in of positions 1a and 1b) (Image Credit: STScI, A. Koekemoer, T. Li).

STATISTICAL PROPERTIES OF THE LARGE SCALE STRUCTURES:

LYMAN-α FOREST

For a review: https://arxiv.org/pdf/1512.00086.pdf

THE LYMAN-α FOREST

Absorption spectra of distant luminous quasars (QSOs) provide a means to probe the properties of the intergalactic medium at high redshift through the analysis of the so called Ly-α forest.
The UV light of a distant quasar – in the wavelengths blue-wards of the Ly-α emission line, λ < 1216Å – traversing the IGM towards the observer could be absorbed by intervening bunches of neutral hydrogen atoms once the photons are redshifted – due to cosmic expansion – to the proper transition frequency. The Ly-α forest, that is the series of absorption features observed in QSOs spectra at wavelengths corresponding to 1216 $(1 + z_a)$ Å, where z_a is the redshift of the absorbers, can be used to map the distribution of the IGM, which is a biased tracer of the underlying DM distribution.
Therefore, the clustering statistics of the flux can be used to constrain the shape and amplitude of the matter power spectrum and measure the structure growth at redshifts 2<z<6, a redshift inaccessible to other LSS probes such as cosmic shear or clusters.

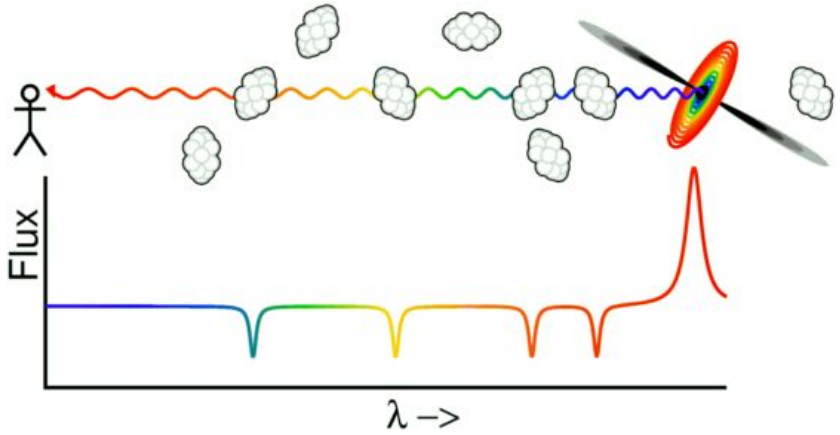

THE LYMAN-α FOREST

Ly-α optical depth:

$$\tau_{\mathrm{Ly}\alpha}(z) = 1.3\,\Delta_b \left(\frac{x_{\mathrm{HI}}}{10^{-5}}\right)\left(\frac{1+z}{4}\right)^{3/2}\left(\frac{dv/dx}{H(z)/(1+z)}\right)^{-1}$$

$\propto$ Baryon density

Fraction of neutral hydrogen

The "trees" in the forest are the highly photoionized sheets, filaments, and halos that result from cosmic structure formation

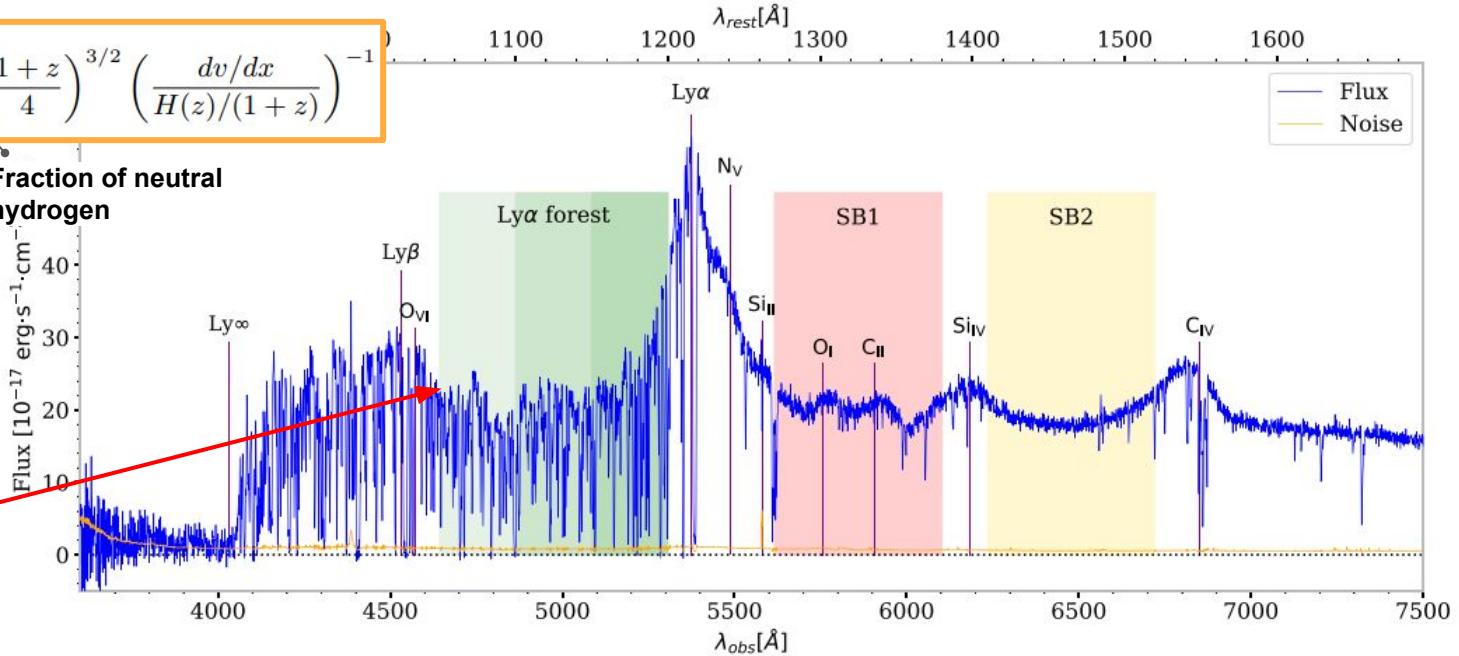

Figure 1. A particularly high-signal spectrum of a quasar located at a redshift $z = 3.42$ measured by DESI with an exposure time of 2300 s. This quasar was observed on 2021 April 12, in the SV3 programme, on DESI tile 221 (TARGETID $= 39627746095137037$, RA $= 217.263°$, Dec. $= -1.755°$). The quasar flux is represented in blue and its noise in orange. The Ly α forest is shown in green. The side-band regions 1 and 2 pictured in red and yellow are used to estimate the forest contamination by metals.

THE LYMAN-α FOREST 1d POWER SPECTRUM

The fluctuations of the Ly α forest flux, δ_f = F(x)/<F(x)> -1, along the line of sight *L,* can be used to measure the one-dimensional (1D) Ly-α forest power spectrum:

$$P_F(k) \equiv \frac{|\tilde{\delta}_f(k)|^2}{L}$$

Cosmological inference from the Lyα forest spectra is complicated by there being no reliable analytic model for the mildly nonlinear densities probed by the forest. All analyses require a comparison with large cosmological simulations.

Above k ≃ 0.02 s/km sensitive to the "warmness" of the dark matter

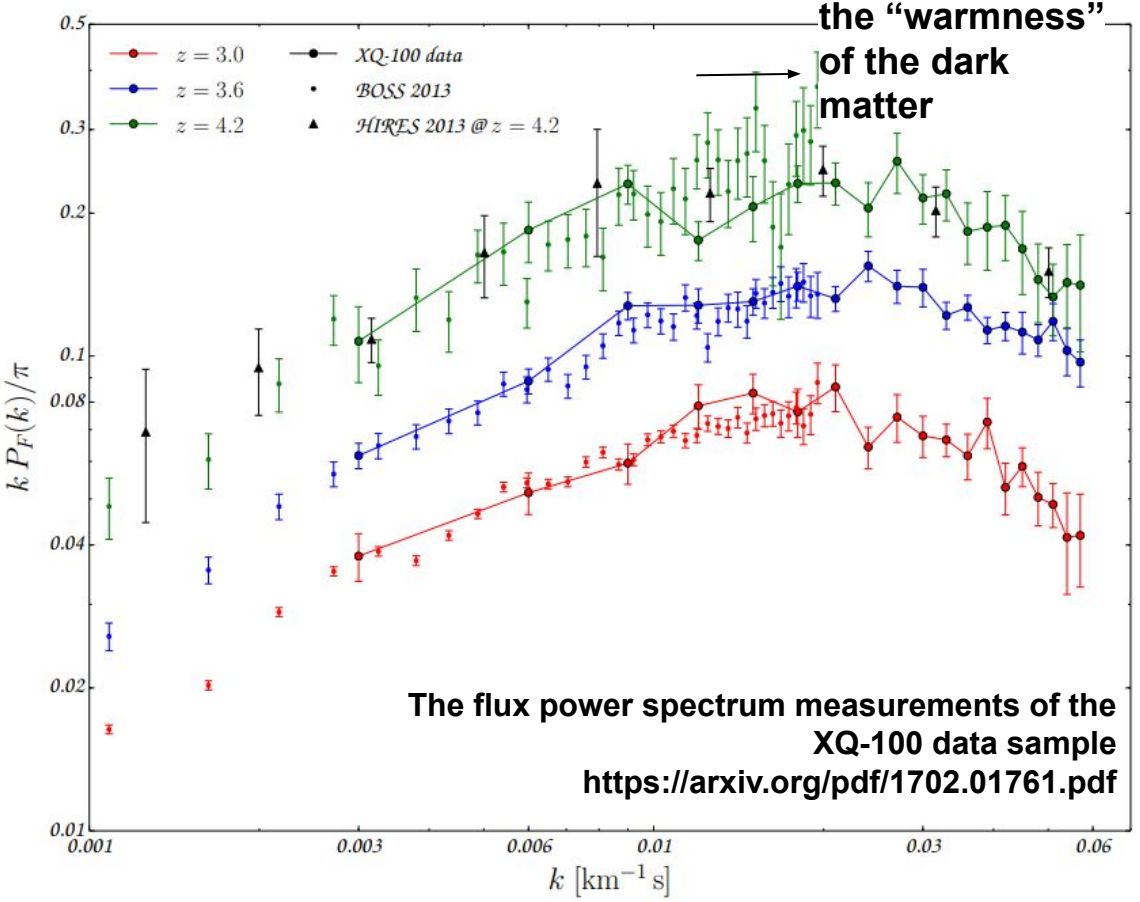

The flux power spectrum measurements of the XQ-100 data sample
https://arxiv.org/pdf/1702.01761.pdf

THE LYMAN-α FOREST 1d POWER SPECTRUM

DESI DR1 Lyα forest: 3D full-shape analysis and cosmological constraints (Cuceo+25)

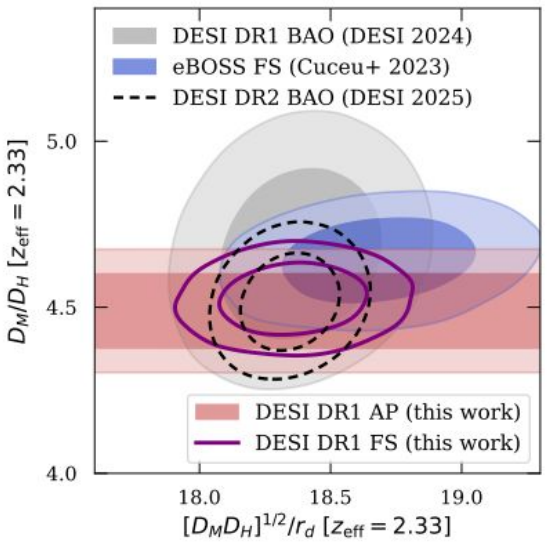

Figure 11. Constraints on the Alcock-Paczynski parameter given by the distance ratio D_M/D_H, and the distance combination corresponding to our isotropic BAO measurement, $[D_M D_H(z_{\rm eff})]^{1/2}/r_d$. DESI Lyα BAO results are shown in grey for DR1 (DESI24-Lyα) and in black dashed for DR2 (DESI Collaboration et al. 2025c), while the eBOSS Lyα full-shape results from Cuceu et al. (2023a) are shown in blue. Our broadband-only AP constraint is given by the horizontal bands in red, while the full-shape result, which includes broadband AP and BAO information, is shown in purple.

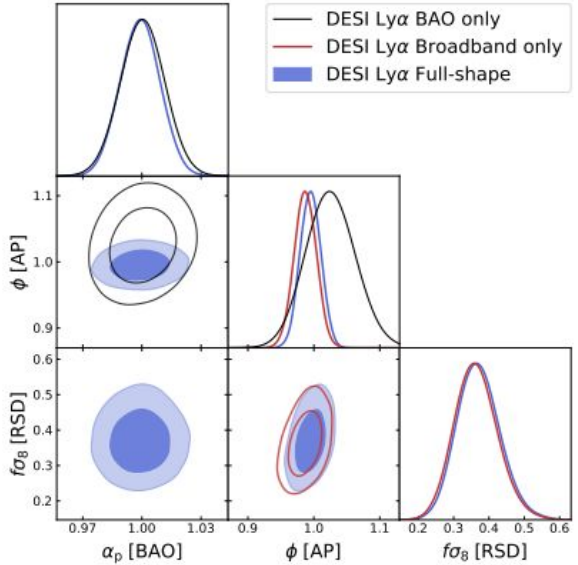

Figure 2. Constraints on the isotropic BAO scale, $\alpha_{\rm p}$, the Alcock-Paczynski effect, ϕ, and the growth parameter combination, $f\sigma_8$. Our main results are shown in blue for the full-shape analysis of the DESI DR1 Lyα forest correlations, where the AP constraint is given by $\phi_{\rm f}$. For comparison, we also show the BAO measurement measured by DESI24-Lyα from the same dataset in black (AP given by $\phi_{\rm p}$), and results from only the broadband in red (where we marginalize over BAO and AP is given by $\phi_{\rm s}$). The Alcock-Paczynski constraint from the broadband is more than a factor of two tighter than the one from BAO.

STATISTICAL PROPERTIES OF THE LARGE SCALE STRUCTURES:

21cm COSMOLOGY

For a review: https://iopscience.iop.org/article/10.1088/1742-6596/956/1/012003/pdf
https://arxiv.org/pdf/2203.17039
https://arxiv.org/pdf/2602.03011

21-CM RADIATION

21-cm radiation originates from the hyperfine transition (spin-flip) of the hydrogen atom:

- **Strongly forbidden line, $t_{1/2}$ ~10^7 yr**
- **HI very abundant**
- **Spectrally isolated**
- **Small obscuration**
- **Earth's atmosphere is transparent to radio frequencies**

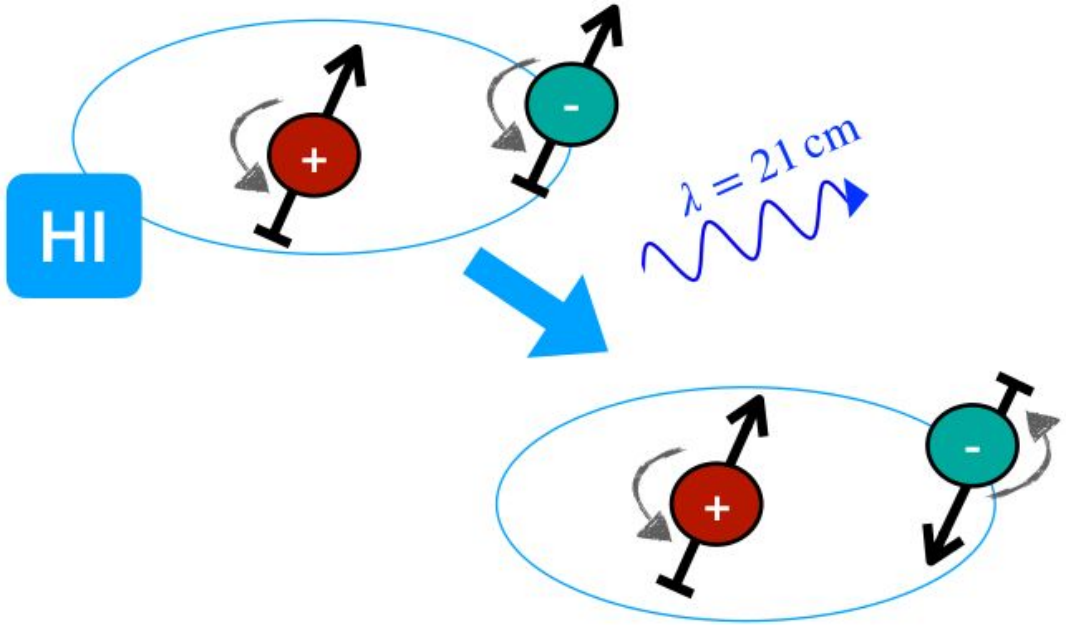

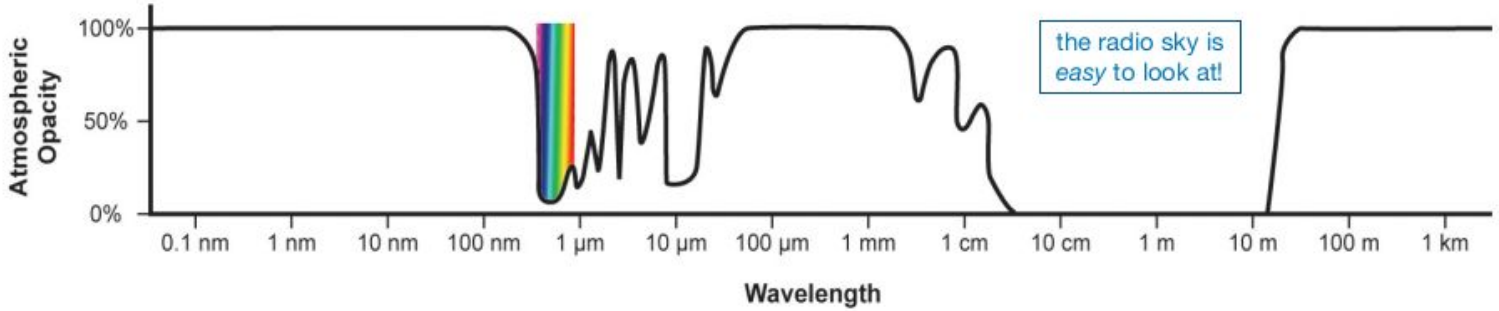

21-CM RADIATION FROM NEARBY GALAXIES

Assuming that the hydrogen atoms are uniformly distributed throughout galaxies, each line of sight through the galaxy will reveal a hydrogen line. The only difference between each of these lines is the Doppler shift that each of these lines has.

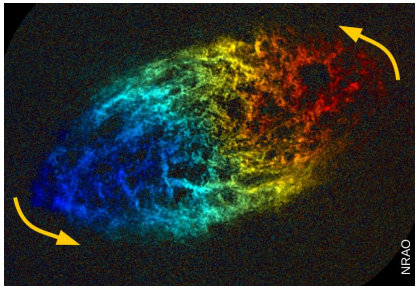

Observations of the hydrogen line have been used to reveal the spiral shape of the Milky Way and to calculate the mass and dynamics of individual galaxies through their velocity rotation curve.

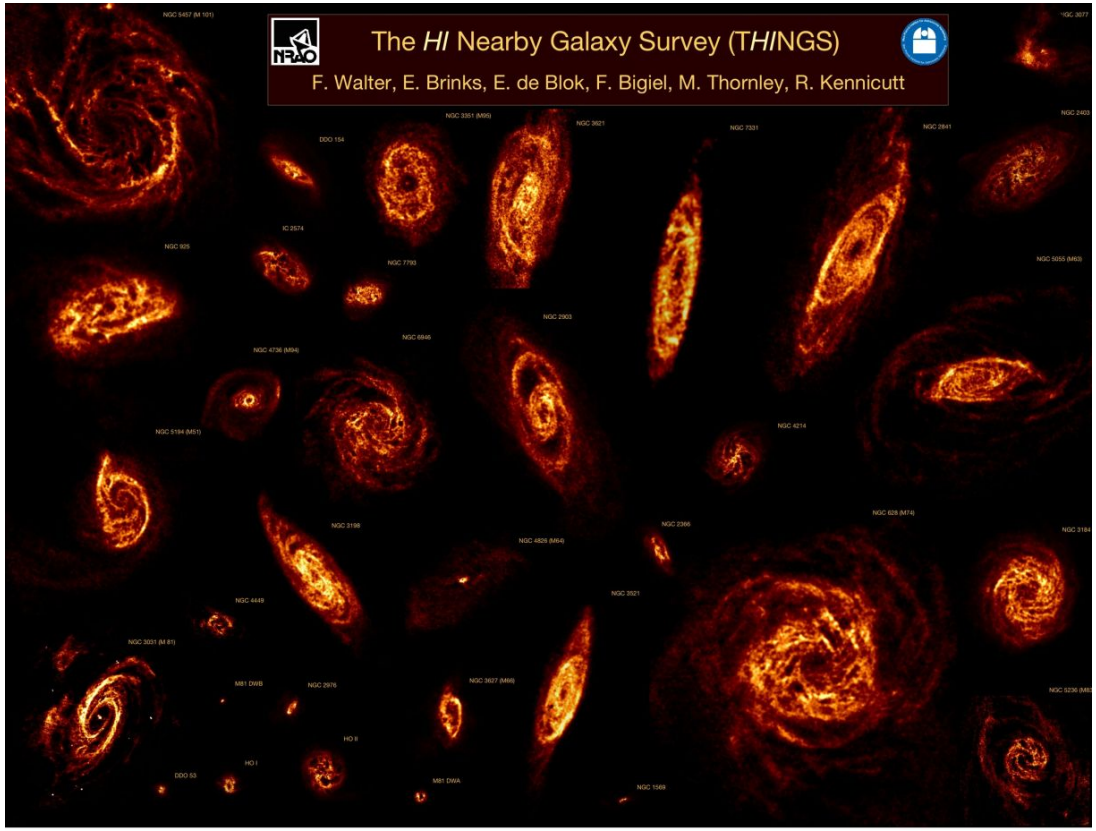

21-CM COSMOLOGY: INTENSITY MAPPING

Intensity mapping is an observational technique for surveying the large-scale structure of the universe by using the integrated radio emission from unresolved HI gas clouds.

The frequency of the emission line is redshifted by the expansion of the Universe, thus the signal can be used to reconstruct the matter density field over cosmic time (tomography).

Intensity mapping surveys can be carried out much faster than conventional optical redshift surveys; it is possible to map-out significantly larger volumes of the Universe.

GALAXY FIELD

HI INTENSITY FIELD

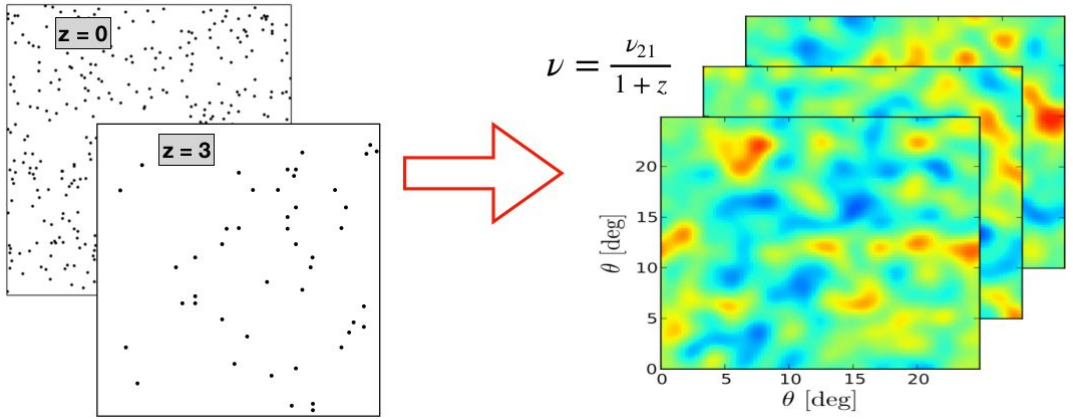

21-CM INTENSITY MAPPING

It can be used to probe the cosmological "dark ages" from recombination (when stable hydrogen atoms first formed) to reionization:

- **It can provide a picture of how the universe was re-ionized: neutral hydrogen which has been ionized by radiation from stars or quasars will appear as holes in the 21 cm background.**

- **By mapping the intensity of redshifted 21 cm radiation – λ = 21cm×(1+z) – it can measure the matter power spectrum in the period after recombination (BAO, RSD, etc, etc).**

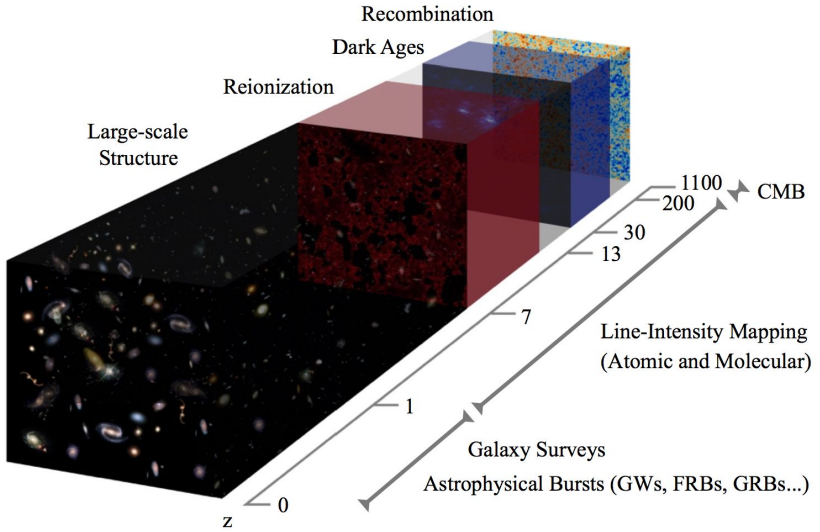

1. Large areas

2. Deep and accurate redshifts (distances)

3. Better coverage of the Universe epochs

21-CM INTENSITY MAPPING POWER SPECTRUM

- **Cosmic HI density** - $\Omega_{HI} \propto \bar{T}_{HI}$ overall amplitude of the power spectrum
- **HI bias** - amplitude plus non-linear scale-dependence
- **HI shot noise** - Poisson noise on the power spectrum depending on number densities
- $P_{HI}(k) = \bar{T}_{HI} b_{HI} P_{DM} + \mathrm{SN}$

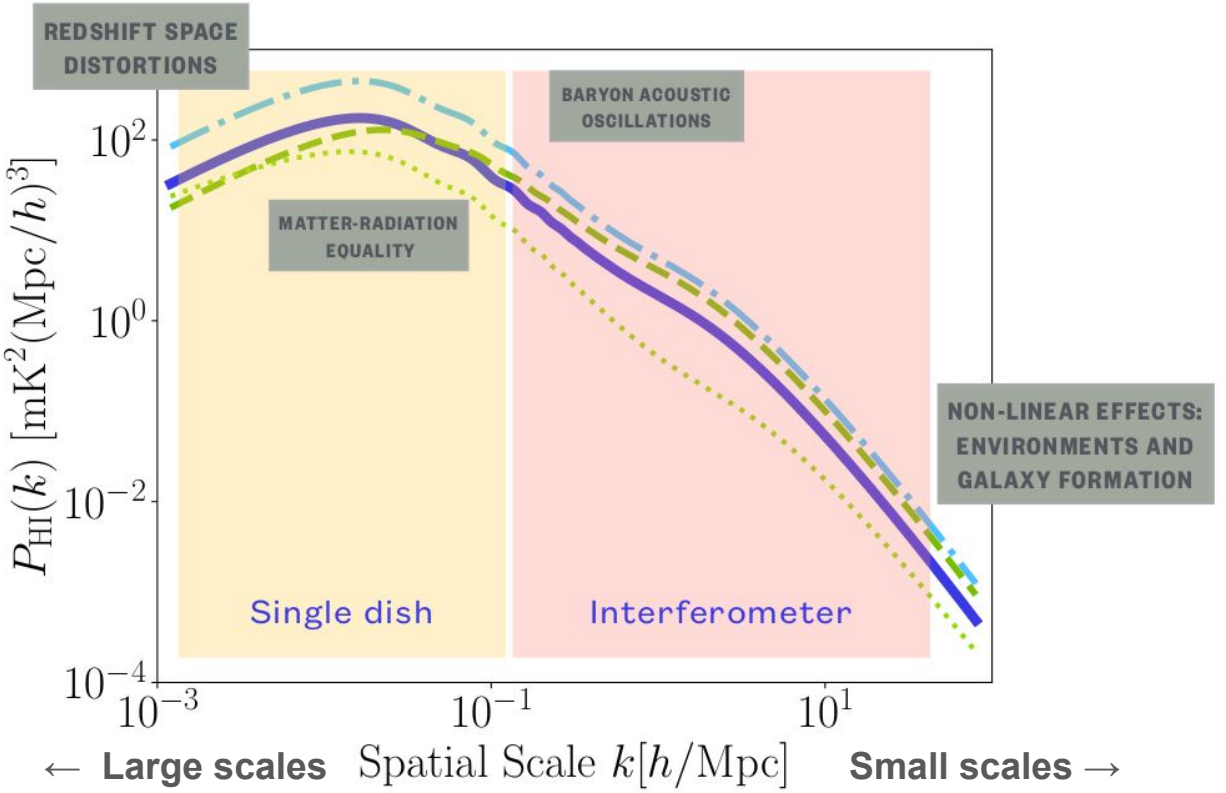

SQUARE KILOMETER ARRAY OBSERVATORY

SKAO

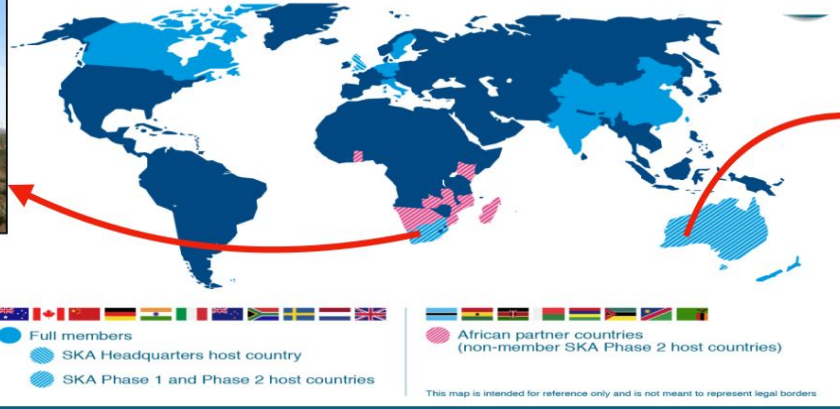

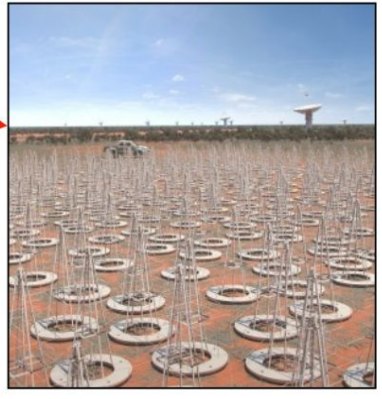

SKA1-mid
the SKA's mid-frequency instrument

0 < z < 3

Frequency range:
350 MHz
to
15.3 GHz
with a goal of 24 GHz

197 dishes
(including 64 MeerKAT dishes)

Maximum baseline:
150km

SKA1-low
the SKA's low-frequency instrument

3 < z < 27

Frequency range:
50 MHz
to
350 MHz

~131,000
antennas spread between
512 stations

Maximum baseline:
~65km

SQUARE KILOMETER ARRAY OBSERVATORY

Wide Survey of 20,000 deg² at 0.35-1.05 GHz for
- Continuum galaxy survey with ~100 million objects
- HI intensity maps for 0.35<z<3

Deep Survey 100 deg² at 200-350 MHz for
- HI intensity maps for 3<z<6

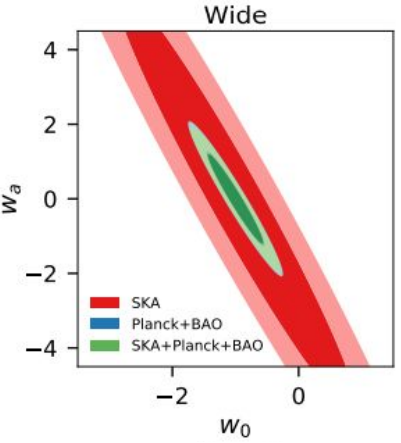

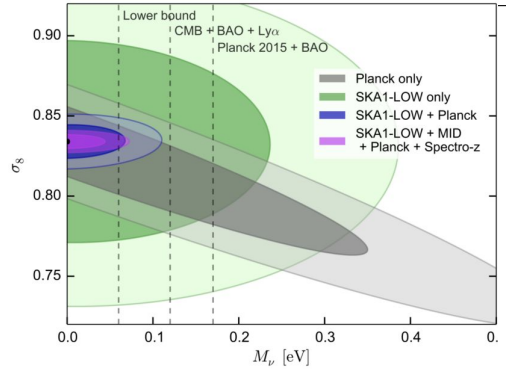

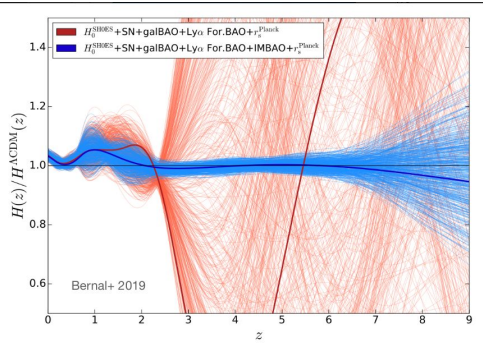

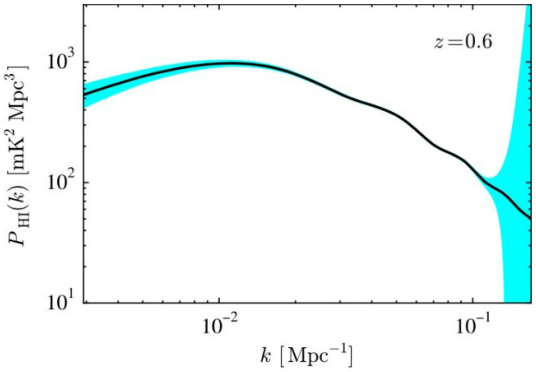

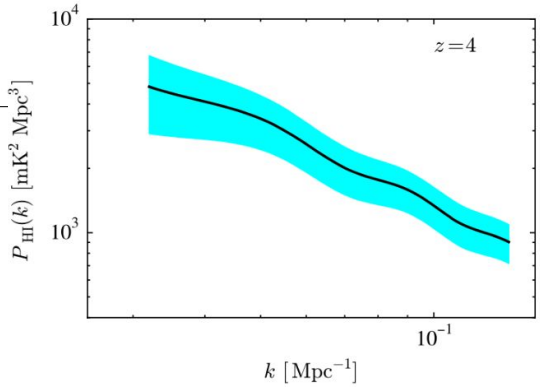

https://arxiv.org/abs/1811.02743

21-CM INTENSITY MAPPING

CHALLENGES:

The IM signal is weak compared to the contaminants

- **Receiver Noise: amplitude comparable to signal -> isotropic, 1/f noise can be removed, manageable in power spectrum space**
- **Instrumental errors: calibration uncertainties, sidelobes, pointing errors, polarization leakage**
- **Radio Frequency Interference: contaminates in spatial and frequency space -> go to the desert, stay away from satellites**
- **Foreground contaminations: Galactic emission and extra-Galactic point sources**

SIGNAL INTENSITY

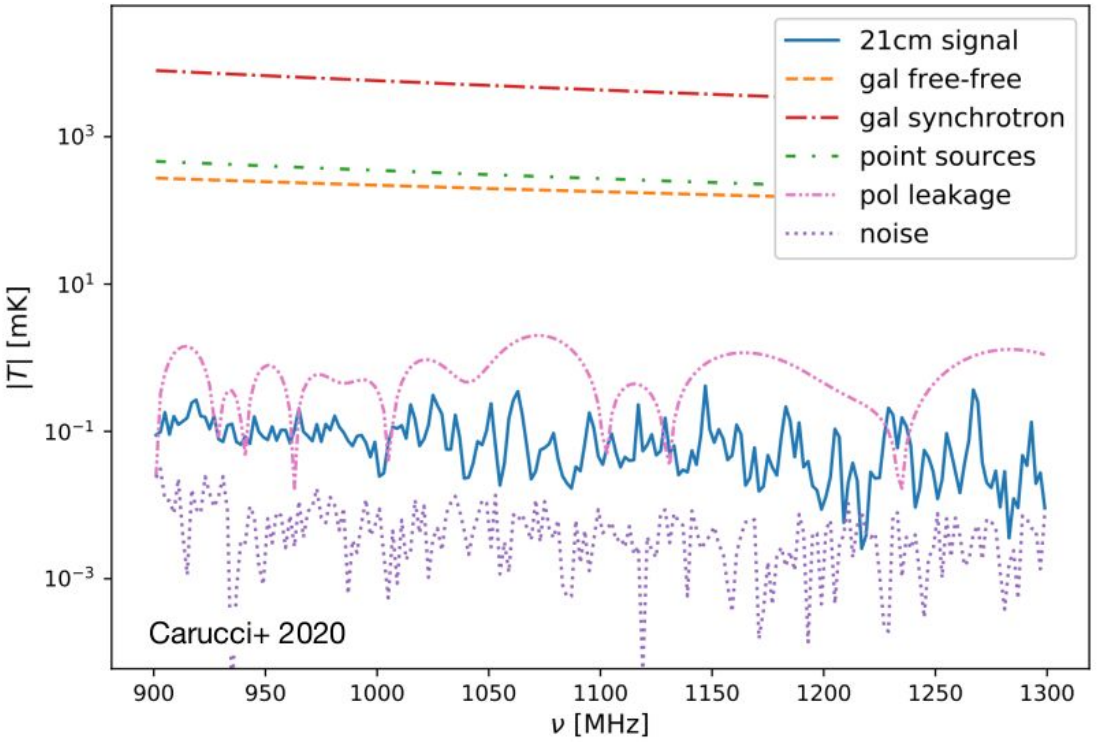

COSMOLOGY WITH GRAVITATIONAL WAVES

For a review: http://arXiv.org/abs/0903.0338v1

https://wwwmpa.mpa-garching.mpg.de/~komatsu/lecturenotes/Azadeh_Maleknejad_on_GW.pdf

https://onlinelibrary.wiley.com/doi/10.1002/andp.202200180

https://arxiv.org/pdf/2502.00239

MULTI-MESSENGER COSMOLOGY

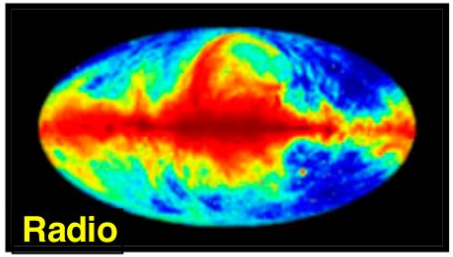

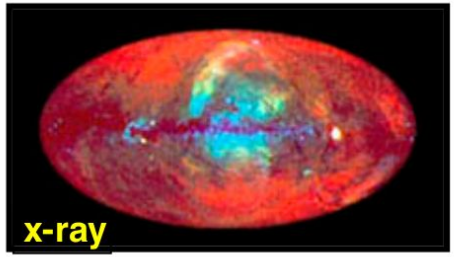

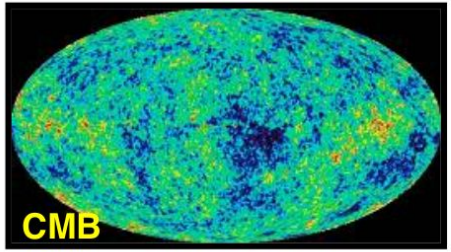

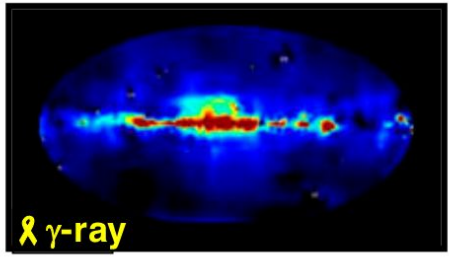

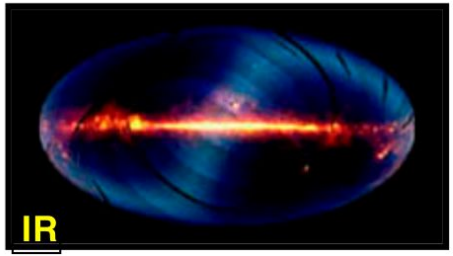

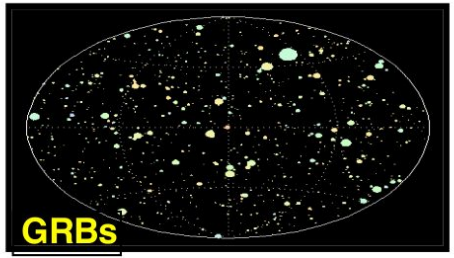

Most of what we know about the Universe is through photons.

Lots of ongoing efforts to obtain information about the universe using non-EM cosmic messengers.

MULTI-MESSENGER COSMOLOGY: COSMIC NEUTRINOS

First detection from Supernova 1987 by IMB , Kamioka (2002 Nobel prize M. Koshiba)

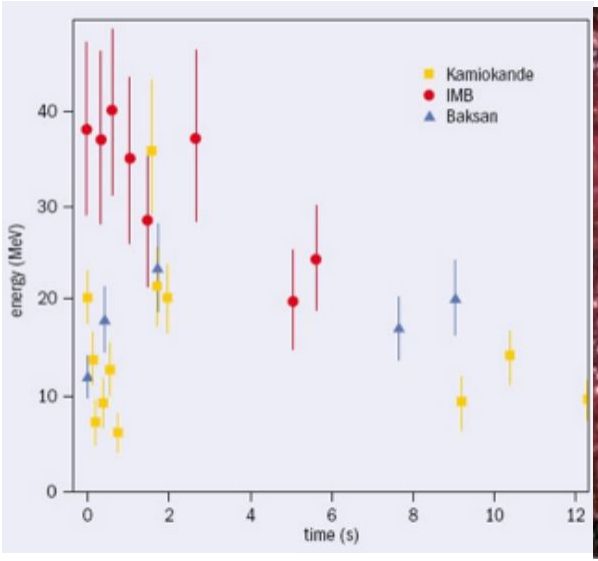

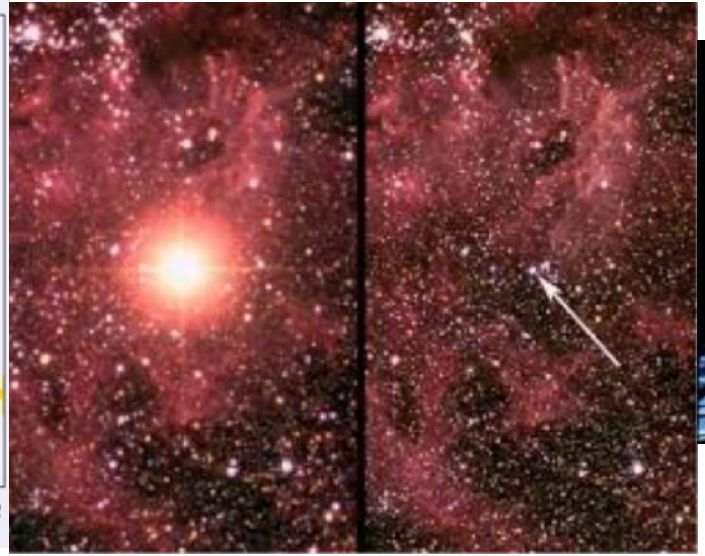

IMB detector

MULTI-MESSENGER COSMOLOGY: COSMIC NEUTRINOS

The IceCube Neutrino Observatory, located at the South Pole, is designed to detect high energy (≳1 TeV) astrophysical neutrinos and identify their sources. Neutrinos are detected through Cherenkov radiation, emitted by charged secondary particles that are produced by neutrino interactions with nuclei in the ice or bedrock. Because of the large momentum transfer from the incoming neutrino, the directions of secondary particles are closely aligned with the incoming neutrino direction, enabling the identification of the neutrino's origin.

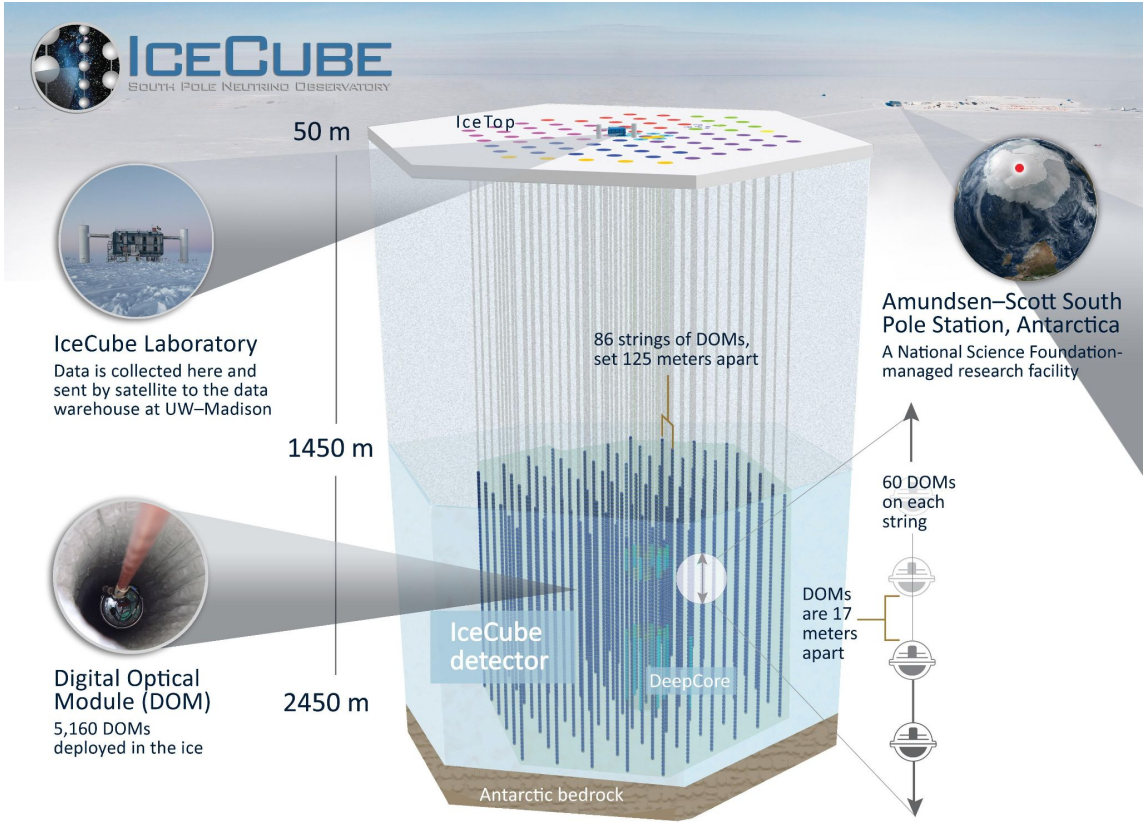

MULTI-MESSENGER COSMOLOGY: COSMIC NEUTRINOS

Extragalactic High-energy neutrinos seen by IceCube Neutrino Observatory

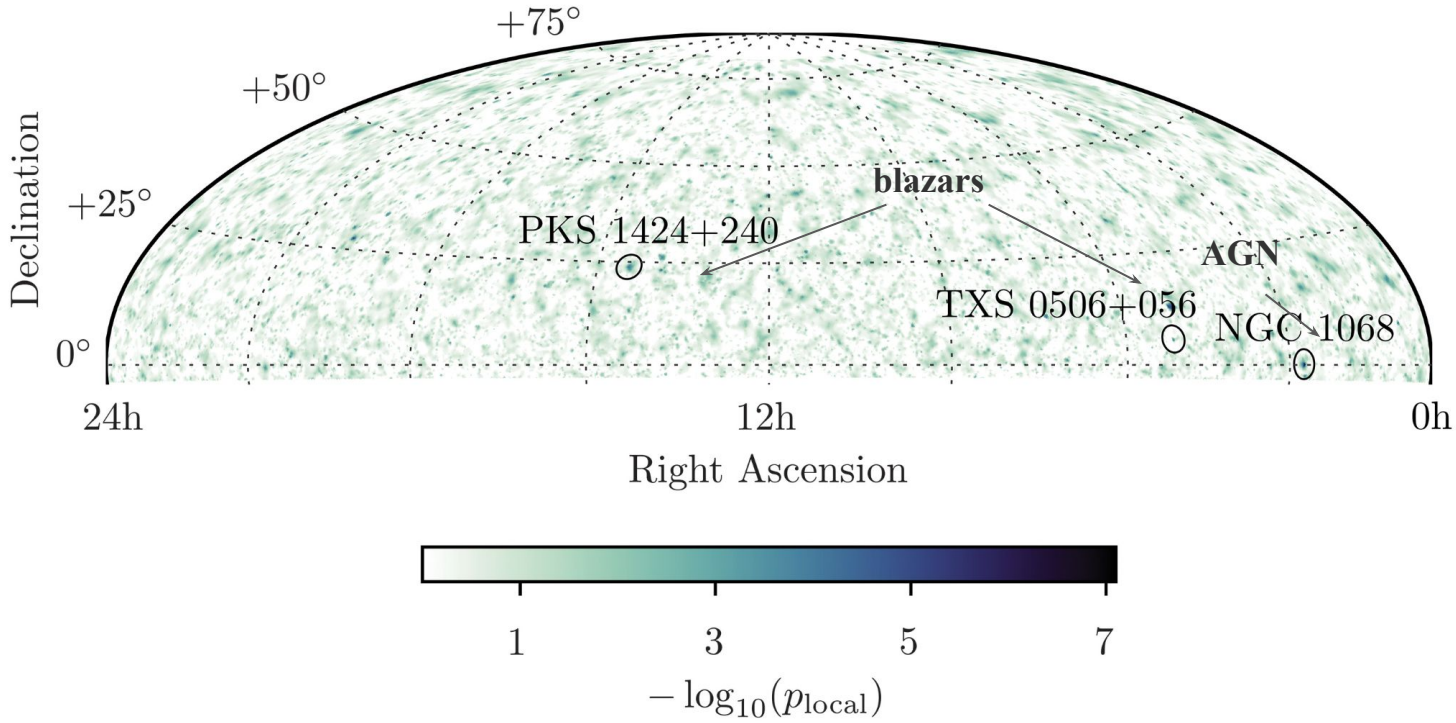

https://www.science.org/doi/10.1126/science.abg3395

MULTI-MESSENGER COSMOLOGY: COSMIC NEUTRINOS

High-energy neutrinos from the MW Galactic plane seen by IceCube Neutrino Observatory

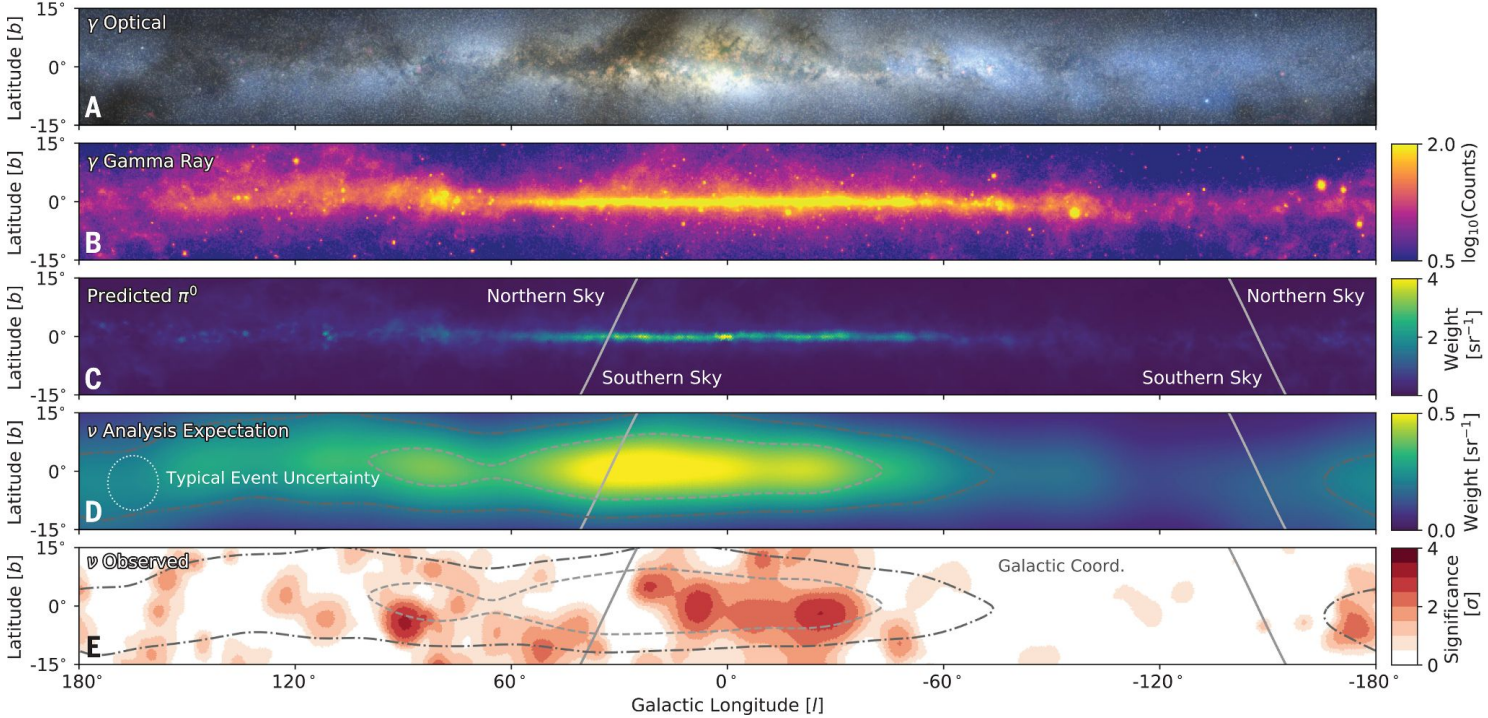

(**A**) Optical color image which is partly obscured by clouds of gas and dust that absorb optical photons. (**B**) The integrated flux in gamma rays from the Fermi Large Area Telescope (Fermi-LAT) 12-year survey at energies greater than 1 GeV,. (**C**) The emission template calculated for the expected neutrino flux, derived from the π0 template that matches the Fermi-LAT observations of the diffuse gamma-ray emission (**D**) The emission template from (C), after including the detector sensitivity to cascade-like neutrino events and the angular uncertainty of a typical signal event (7°, indicated by the dotted white circle). Contours indicate the central regions that contain 20 and 50% of the predicted diffuse neutrino emission signal. (**E**) The pretrial significance of the IceCube neutrino observations, calculated from the all-sky scan for point-like sources by using the cascade neutrino event sample.

https://www.science.org/doi/10.1126/science.adc9818

GRAVITATIONAL WAVES

General Relativity predicts that space-time perturbations propagate through empty space at the speed of light.

$$\left(-\frac{\partial^2}{\partial t^2}+\nabla^2\right)\bar{h}^{\alpha\beta}=0.$$

Two possible polarizations:

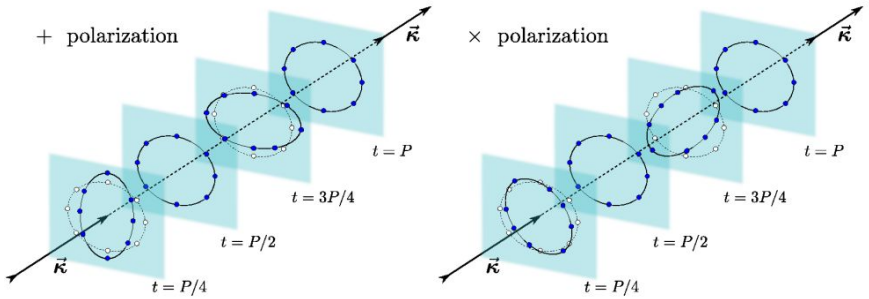

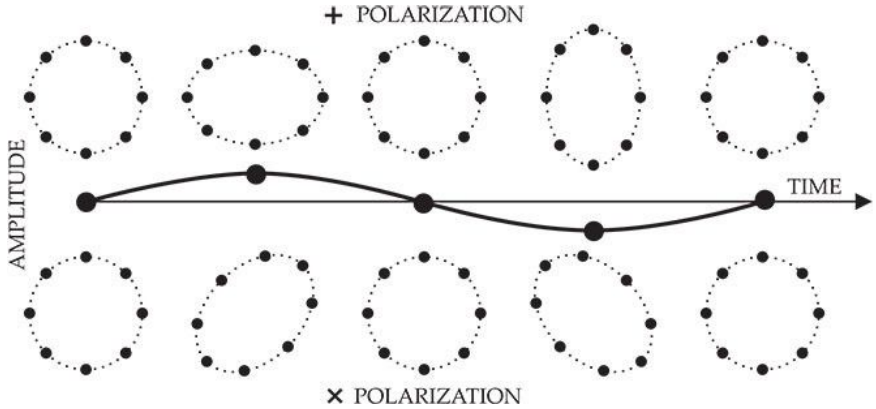

GRAVITATIONAL WAVES

PSR B1913+16: First indirect evidence from orbital period decay of binary system composed of a neutron star and pulsar, a rapidly rotating, highly magnetized neutron star (1993 Nobel prize J. Taylor, R. Hulse): the orbital decay match the energy loss predicted from GR due to gravitational wave radiation.

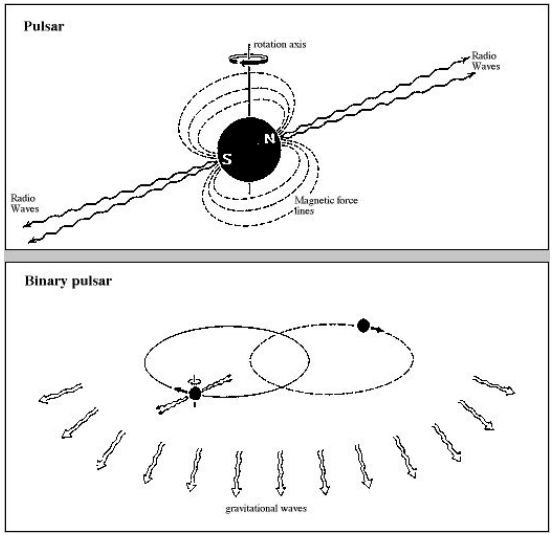

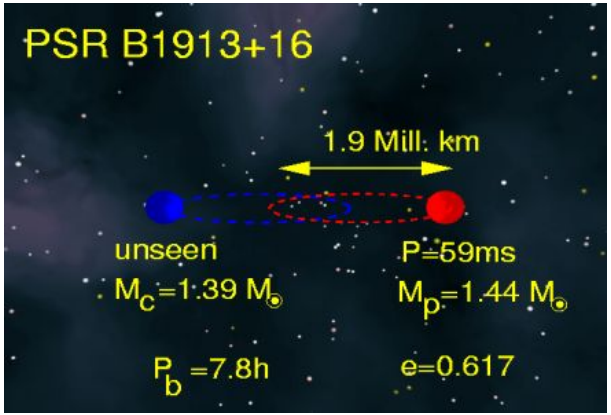

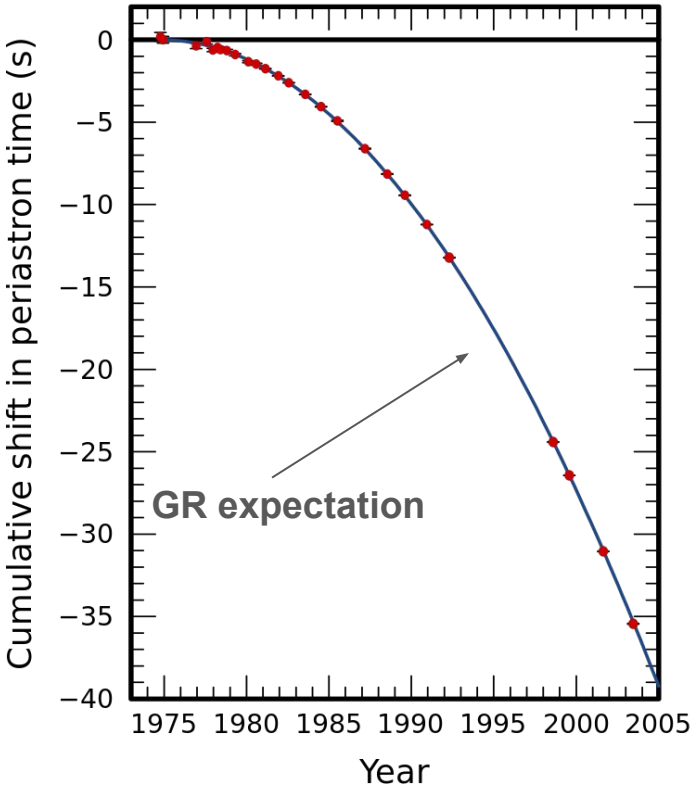

GRAVITATIONAL WAVE SPECTRUM

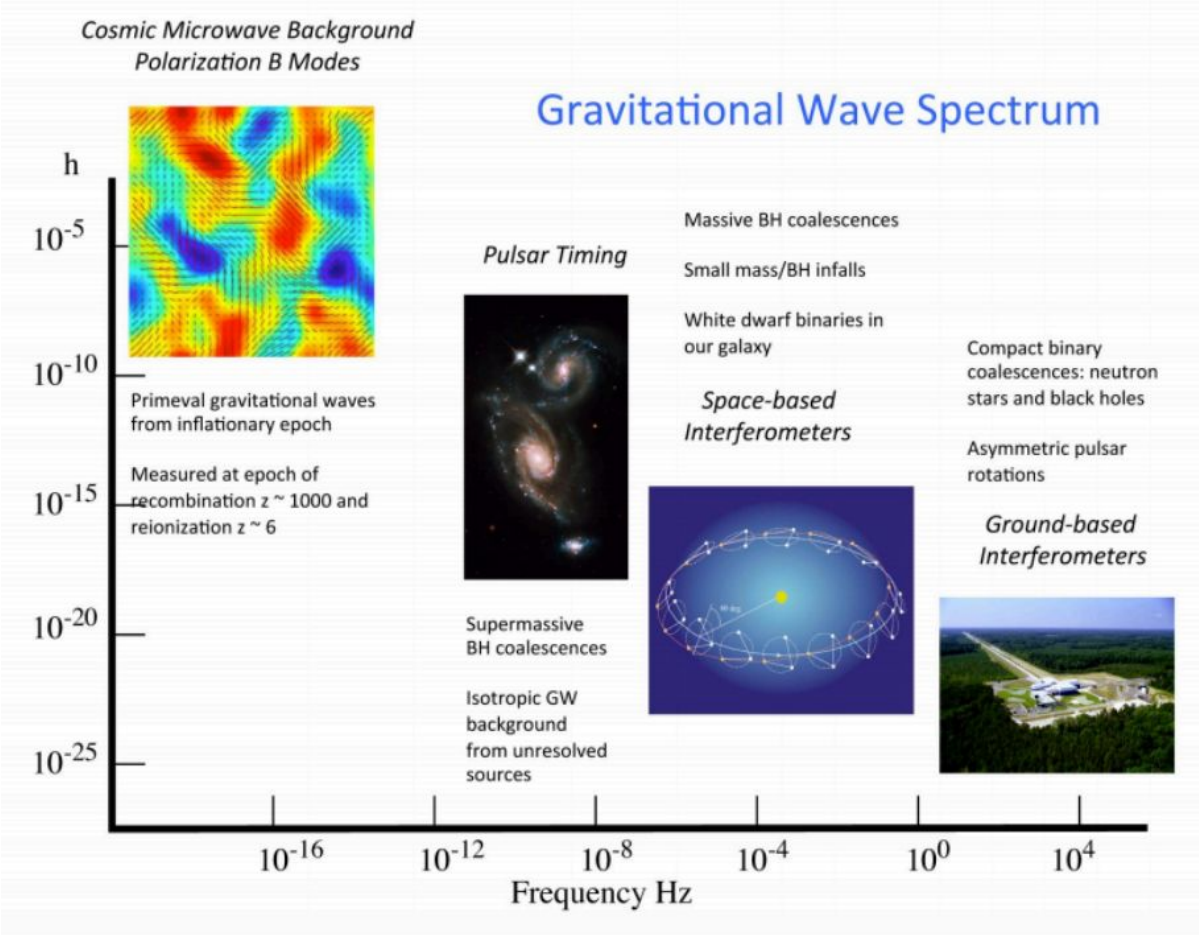

GRAVITATIONAL WAVE INTERFEROMETERS

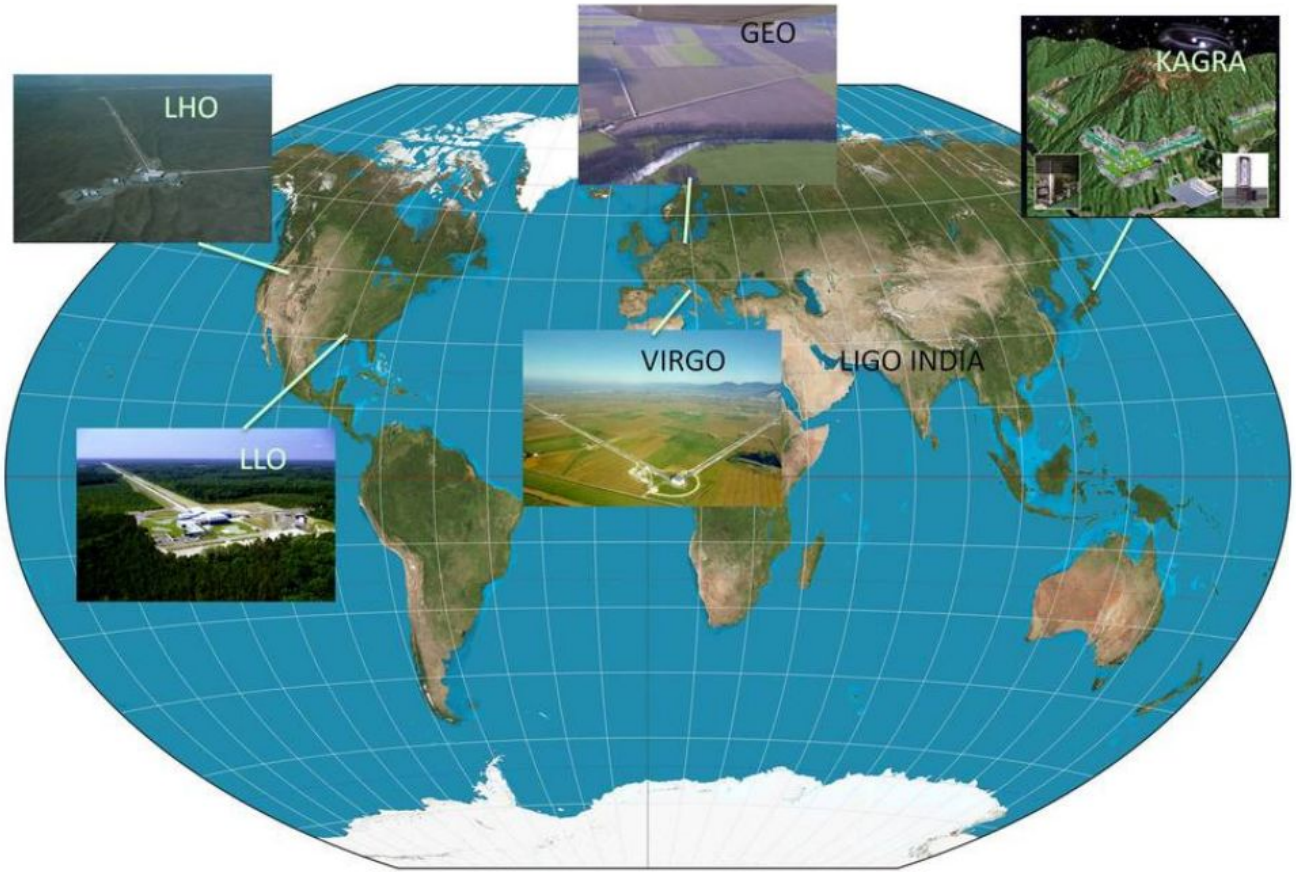

GRAVITATIONAL WAVE INTERFEROMETERS

LIGO & VIRGO Detectors

LIGO observatory contains 2 (H2) km and 4 km (H1) interferometers at Hanford, WA and a 4 km interferometer at Livingston, LA (L1) separated by 3000 km (10ms)

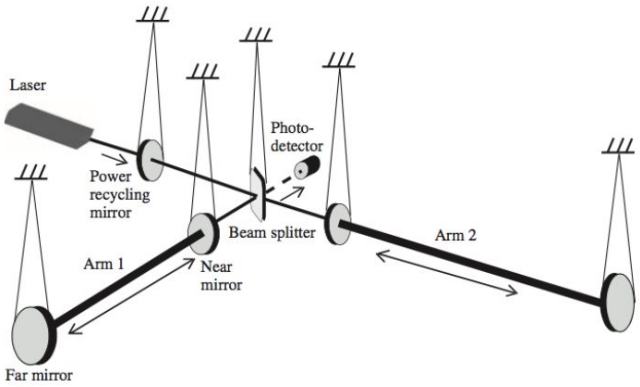

GRAVITATIONAL WAVE INTERFEROMETERS

For a binary system the wave's frequency sweep and amplitude (strain) depend on $\mathscr{M} = (m_1 m_2)^{3/5}/(m_1 + m_2)^{1/5}$, and luminosity distance:

$$\frac{d\Omega}{dt} \propto \left(\frac{G\mathcal{M}}{c^3}\right)^{5/3}$$

$$h \propto \frac{1}{D_L}\left(\frac{G\mathcal{M}}{c^3}\right)^{5/3}\Omega^{2/3}$$

Dimensionless strain, $h = \Delta l/l$, is the main observable measured; the typical relative deformation:

$$h = \frac{\Delta l}{l} \sim 10^{-21}$$

E.g. for the Laser Interferometer Gravitational-Wave Observatory (LIGO):

$l \sim 4\text{km} \rightarrow \Delta l \sim 10^{-16}\text{cm}$

GRAVITATIONAL WAVE INTERFEROMETERS

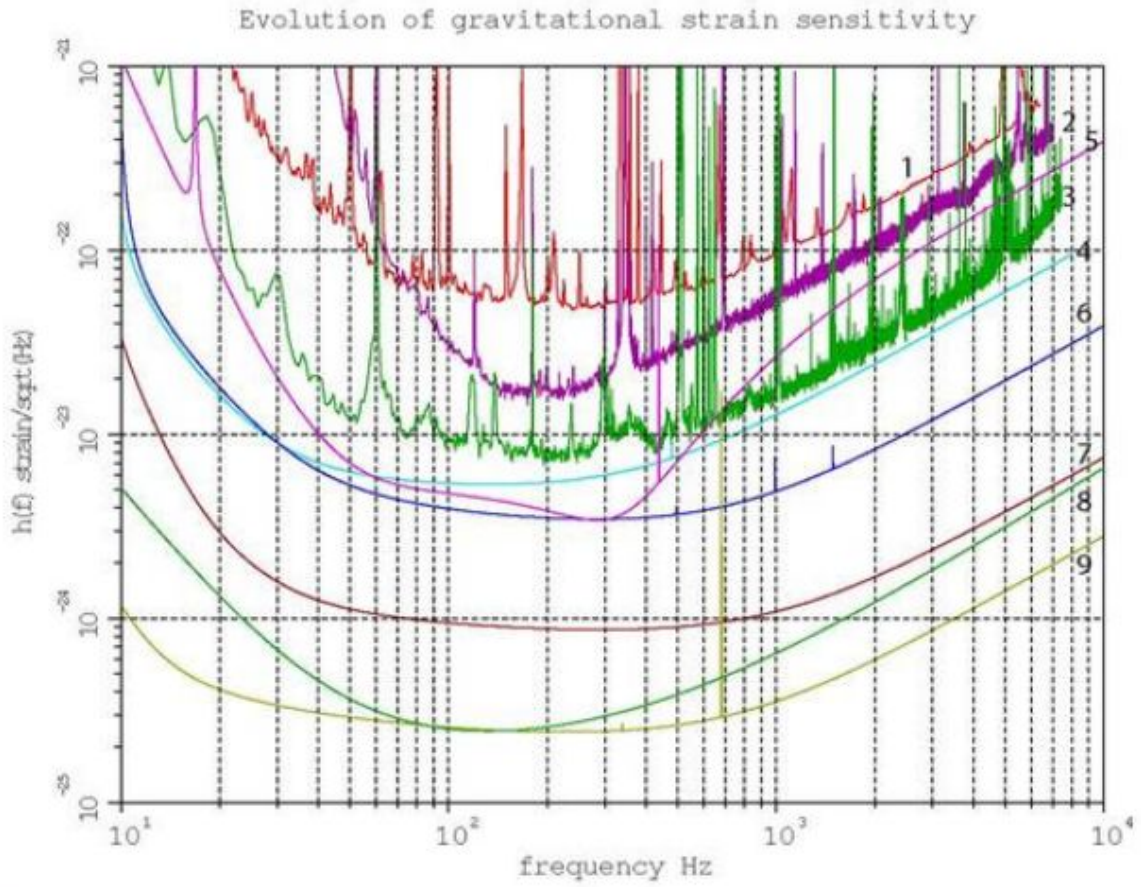

1 VIRGO 2009
2 Enhanced LIGO 2009
3 Advanced LIGO 65Mpc NS/NS 2015
4 Advanced LIGO 150Mpc NS/NS Low Power
5 Advanced VIRGO
6 Advanced LIGO 190Mpc NS/NS High Power
7 4km "Voyager" example 600Mpc NS/NS
8 Einstein telescope B
9 40km "Cosmic Explorer" example

GRAVITATIONAL WAVE INTERFEROMETERS

GW150914: First LIGO detection

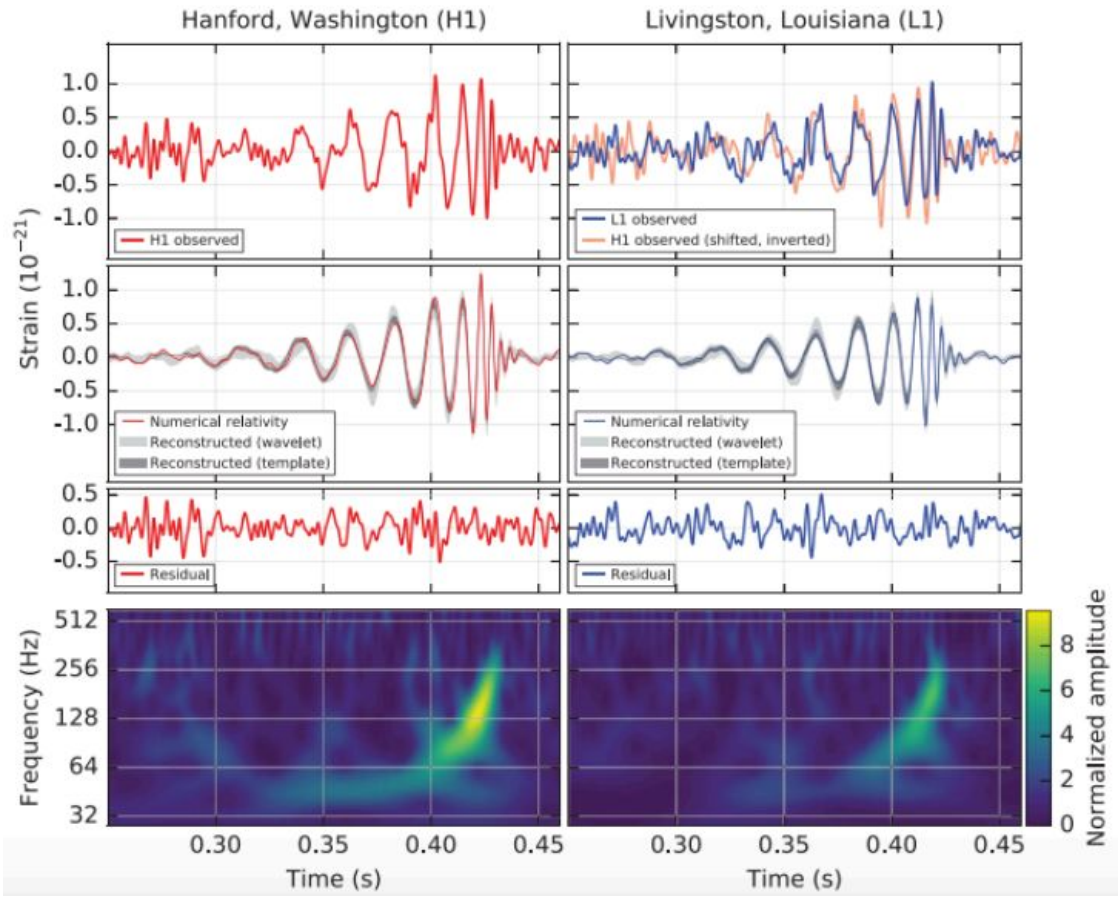

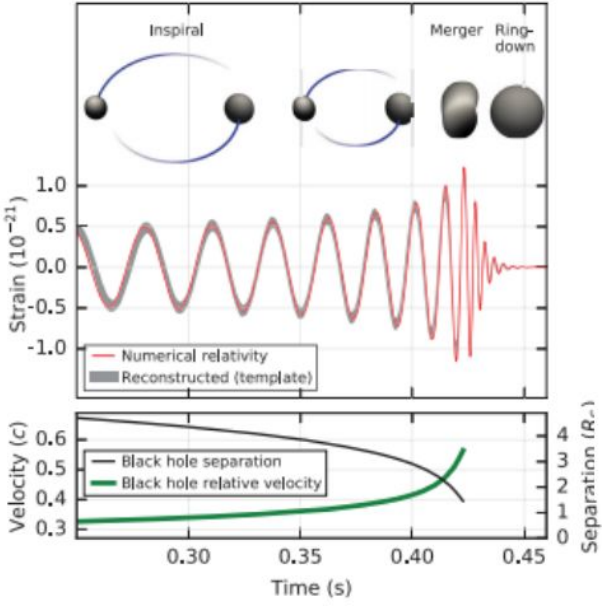

Primary black hole mass	$36^{+5}_{-4} M_\odot$
Secondary black hole mass	$29^{+4}_{-4} M_\odot$
Final black hole mass	$62^{+4}_{-4} M_\odot$
Final black hole spin	$0.67^{+0.05}_{-0.07}$
Luminosity distance	410^{+160}_{-180} Mpc
Source redshift z	$0.09^{+0.03}_{-0.04}$

GRAVITATIONAL WAVE INTERFEROMETERS

Summary of Ligo-Virgo-KAGRA Binary mergers

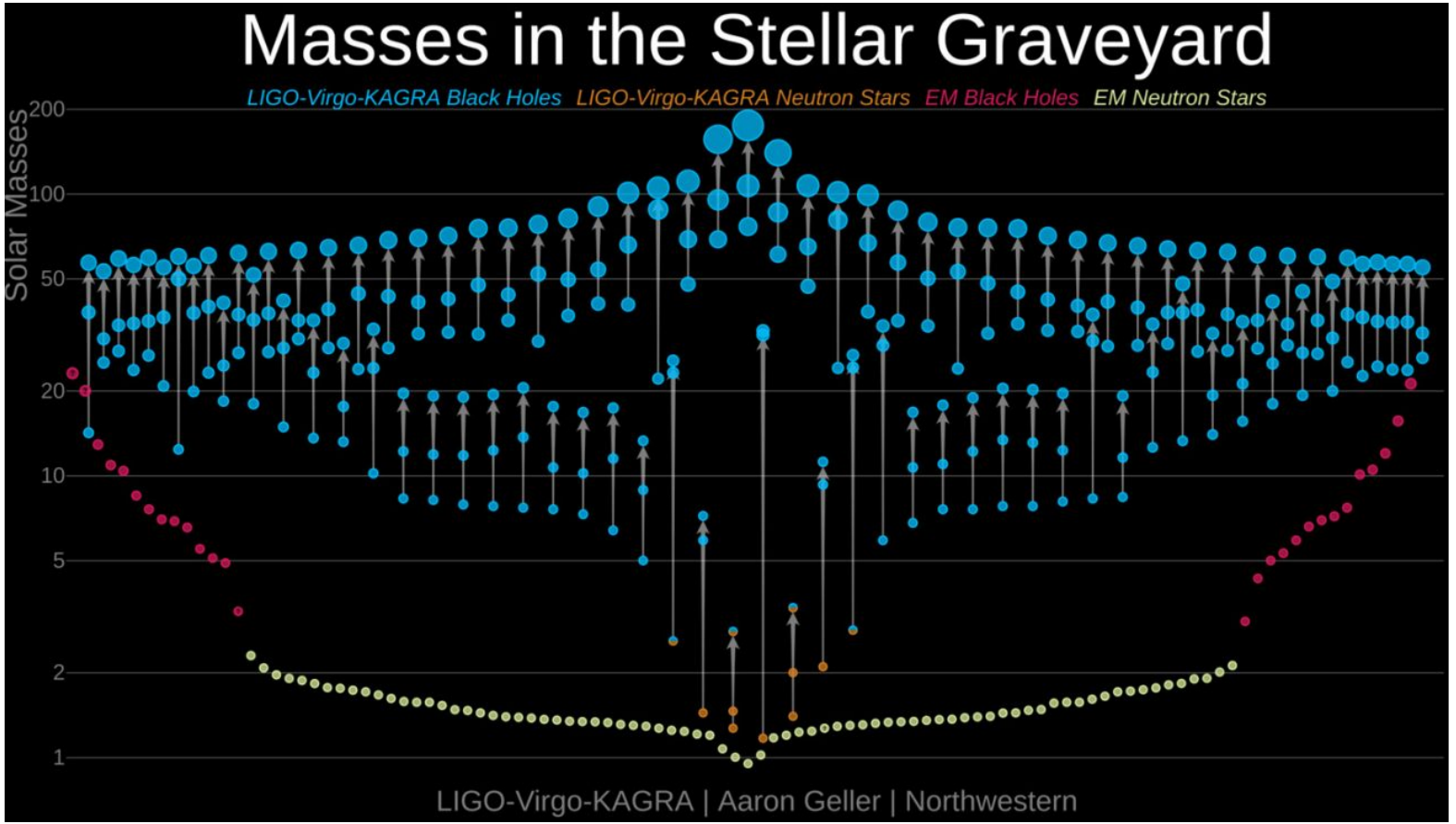

STANDARD SIRENS: GW170817

GW170817: First Binary Neutron star merger

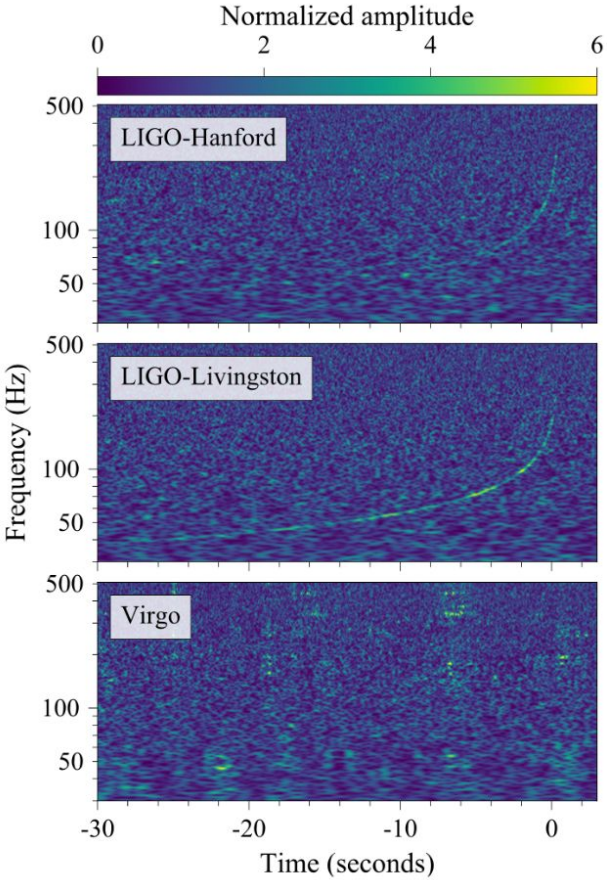

Triangulation of the GW signal:

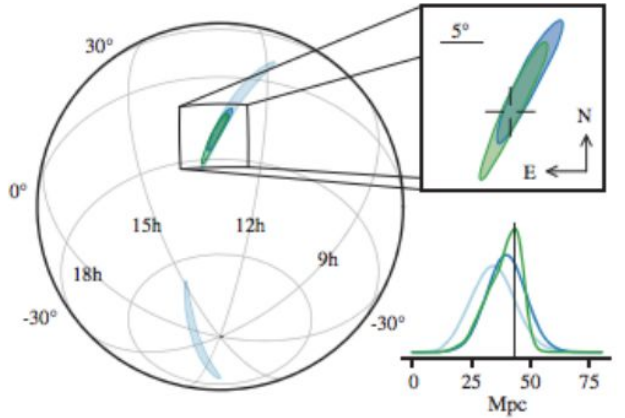

FIG. 3. Sky location reconstructed for GW170817 by a rapid localization algorithm from a Hanford-Livingston (190 deg^2, light blue contours) and Hanford-Livingston-Virgo (31 deg^2, dark blue contours) analysis. A higher latency Hanford-Livingston-Virgo analysis improved the localization (28 deg^2, green contours). In the top-right inset panel, the reticle marks the position of the apparent host galaxy NGC 4993. The bottom-right panel shows the *a posteriori* luminosity distance distribution from the three gravitational-wave localization analyses. The distance of NGC 4993, assuming the redshift from the NASA/IPAC Extragalactic Database [89] and standard cosmological parameters [90], is shown with a vertical line.

STANDARD SIRENS: GW170817

Multi-wavelength follow-up:

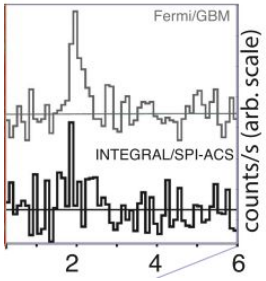

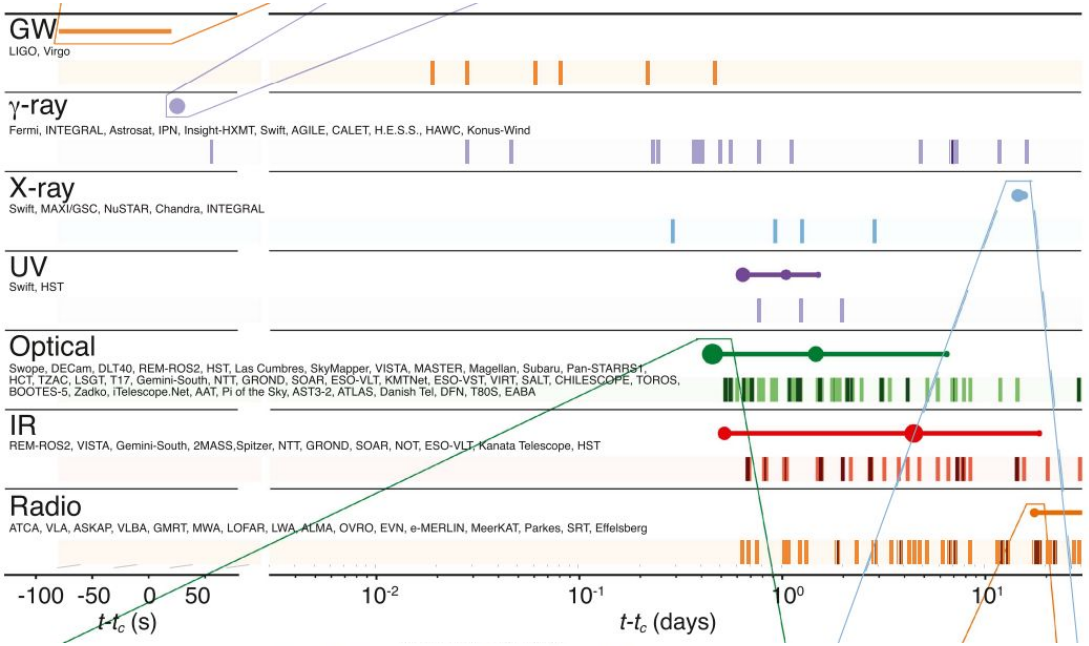

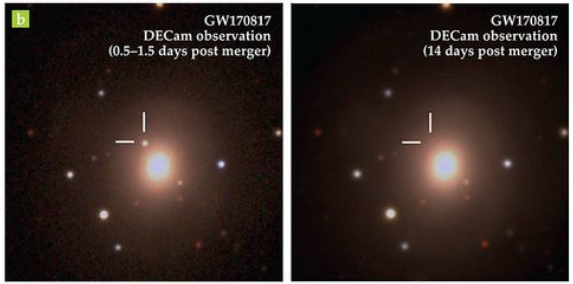

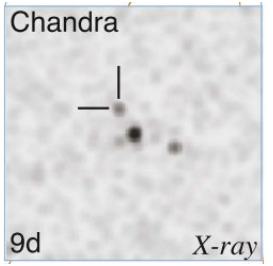

STANDARD SIRENS

- GW are “self-calibrating” sources (Schutz 1986)

$$h \sim D_L^{-1}$$

  - Direct measurement of luminosity distance
  - “Standard sirens”
- In general, no redshift from GWs (Krolak & Schutz 1987)

$$m_{obs} = m_{src}(1+z)$$

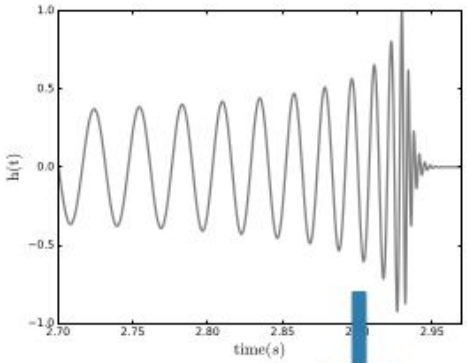

D_L

z

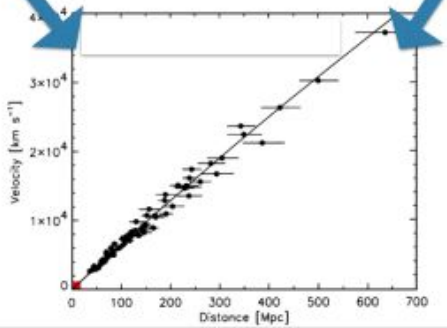

STANDARD SIRENS

- From GW alone

$$D_L = 44^{+3}_{-7}\,\mathrm{Mpc}$$

- NGC 4993

$$z = 0.0098$$

$$H_0 = 70^{+12}_{-8}\,\mathrm{km\,s^{-1}\,Mpc^{-1}}$$

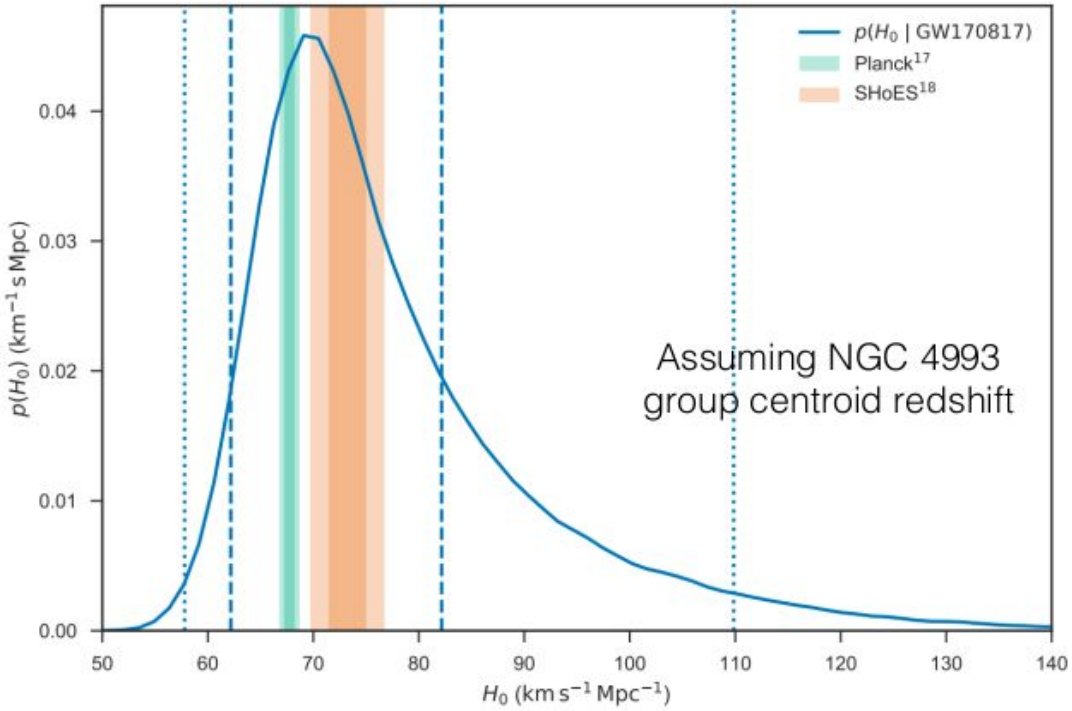

arxiv:1710.05835

DARK STANDARD SIRENS

A dark siren is a gravitational wave event without EM counterpart. Most binary mergers, and in particular binary black hole (BBH) mergers, do not have associated electromagnetic counterparts. However, in the absence of such a counterpart signposting the host galaxy directly, we can still use the gravitational-wave observations to give us information about the sky position of the source – and in this way narrow down the host galaxy to a set of candidate galaxies in this region. Combining redshift information from all of these possible host galaxies then allows us to measure H_0 statistically.

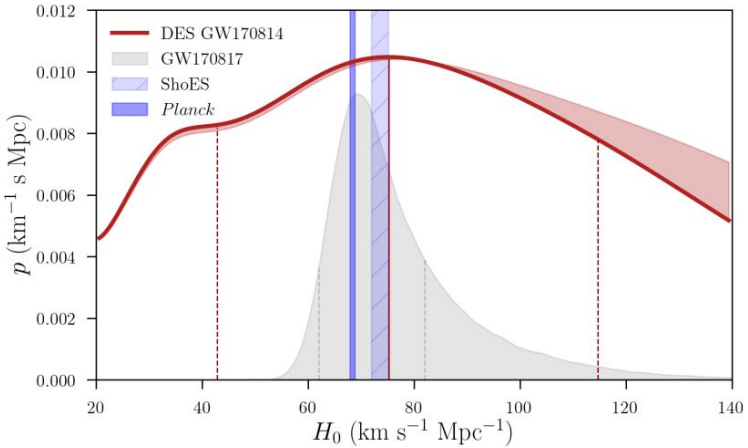

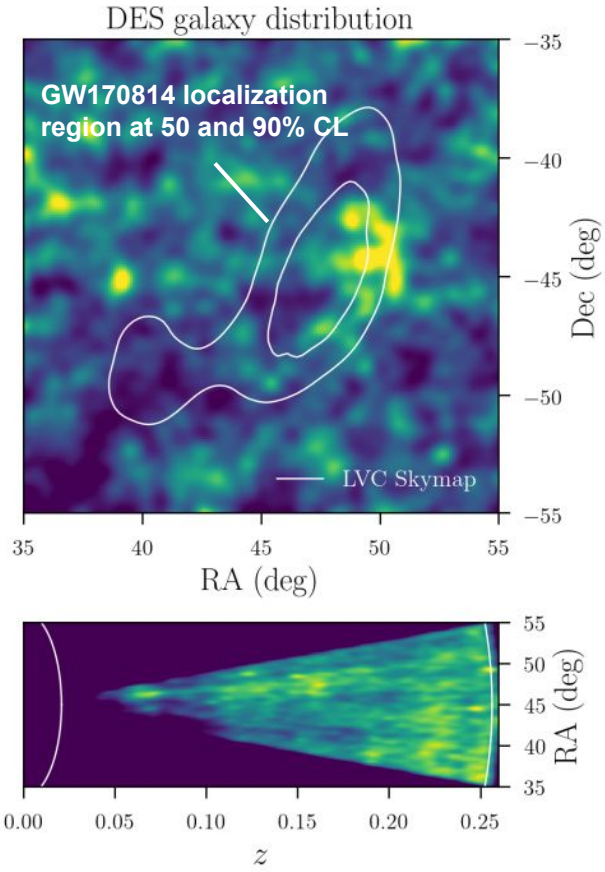

https://arxiv.org/pdf/1901.01540

SPECTRAL SIRENS

Spectral siren cosmology from gravitational-wave observations in GWTC-4.0 Hernandez+25

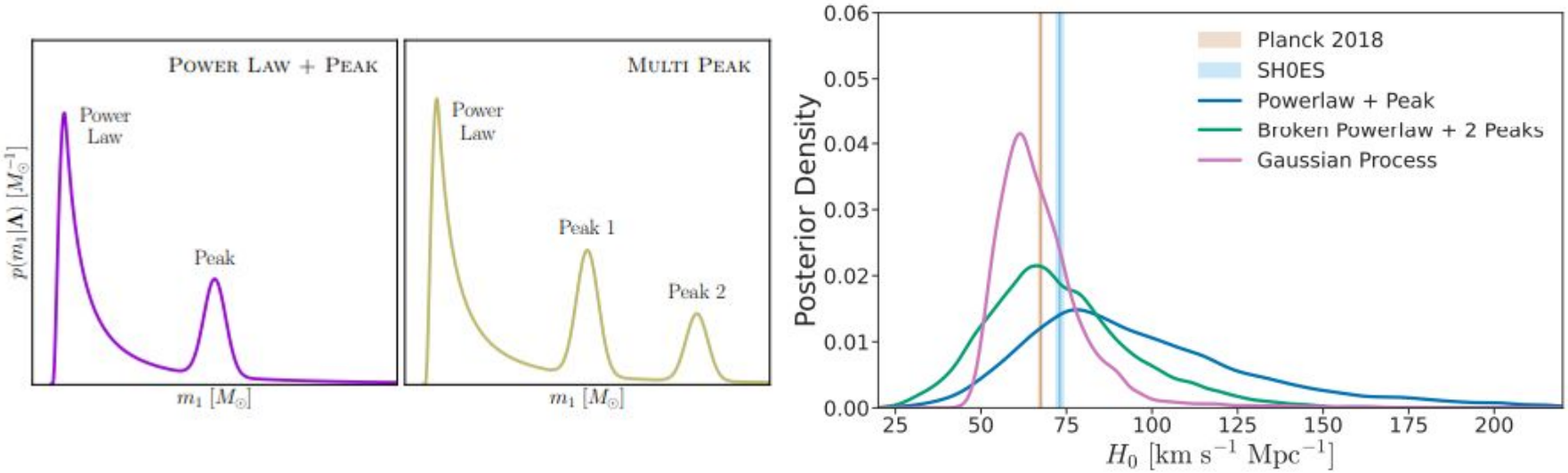

Bright sirens require an electromagnetic counterpart to determine the redshift of the emission source while dark sirens rely on the presence of complete galaxy catalogs over large sky regions. Spectral sirens, using GW data alone, can circumvent these limitations by leveraging features in the mass distribution of compact binaries: Astrophysically motivated models for the source-frame mass distribution of black holes, can be used to statistically infer the redshift of the source and thereby breaking the mass-redshift degeneracy

DARK + SPECTRAL SIRENS

Gravitational-Wave Transient Catalog GWTC-4.0: Constraints on the Cosmic Expansion Rate and Modified Gravitational-wave Propagation https://arxiv.org/pdf/2509.04348

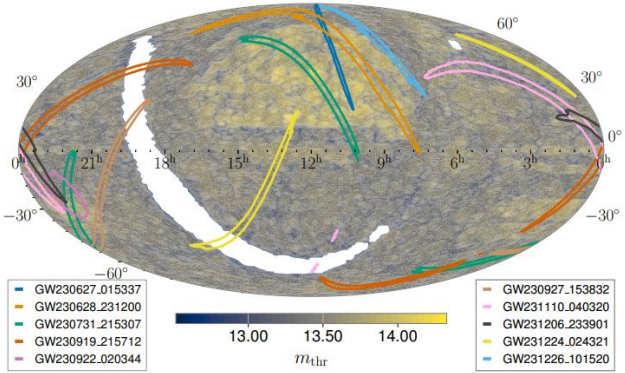

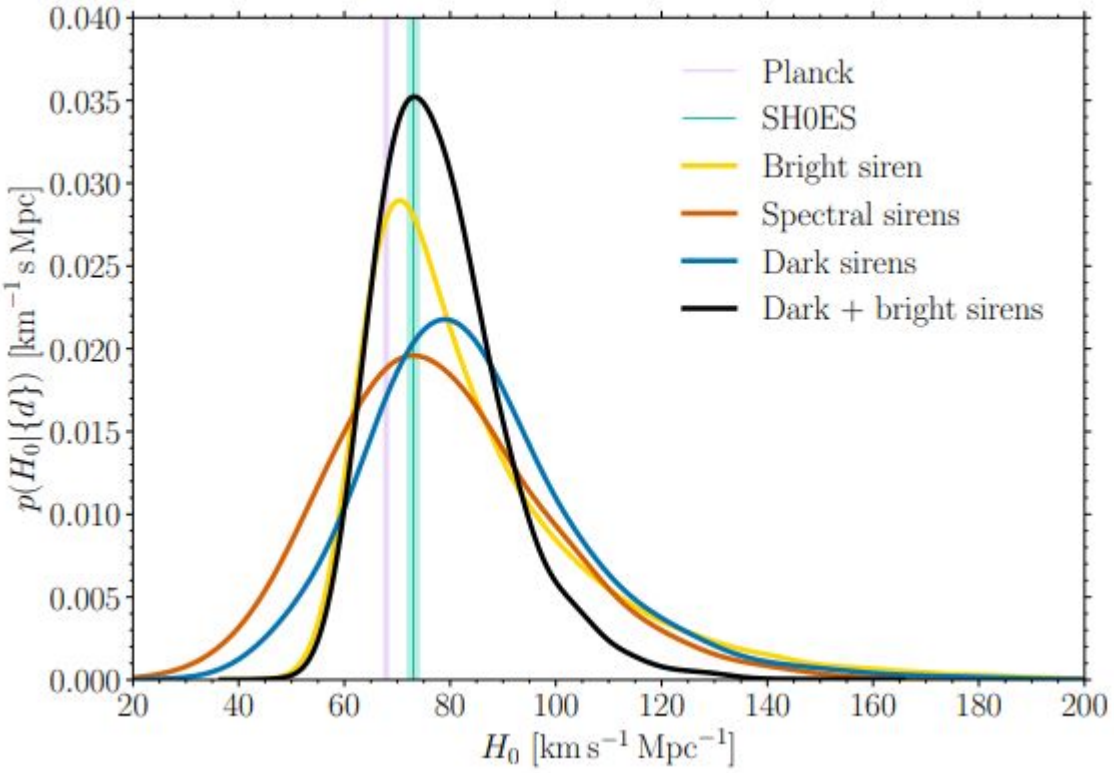

DARK STANDARD SIRENS

Gravitational-Wave Transient Catalog GWTC-4.0: Constraints on the Cosmic Expansion Rate and Modified Gravitational-wave Propagation https://arxiv.org/pdf/2509.04348

Modified gravity can introduce “GW friction”, that is a modifications to the GW amplitude received at the observer. This effect is indistinguishable from a change in the luminosity distance to the GW source. The result is that the luminosity distance D^{GW}_L inferred for a GW source differs from the EM luminosity distance D^{EM}_L.
The ratio D_{GW}/D_{EM} is thus a convenient probe of departures from GR on cosmological scales. The ratio is always equal to one in GR, and in cosmological modified–gravity models can become a function of redshift.

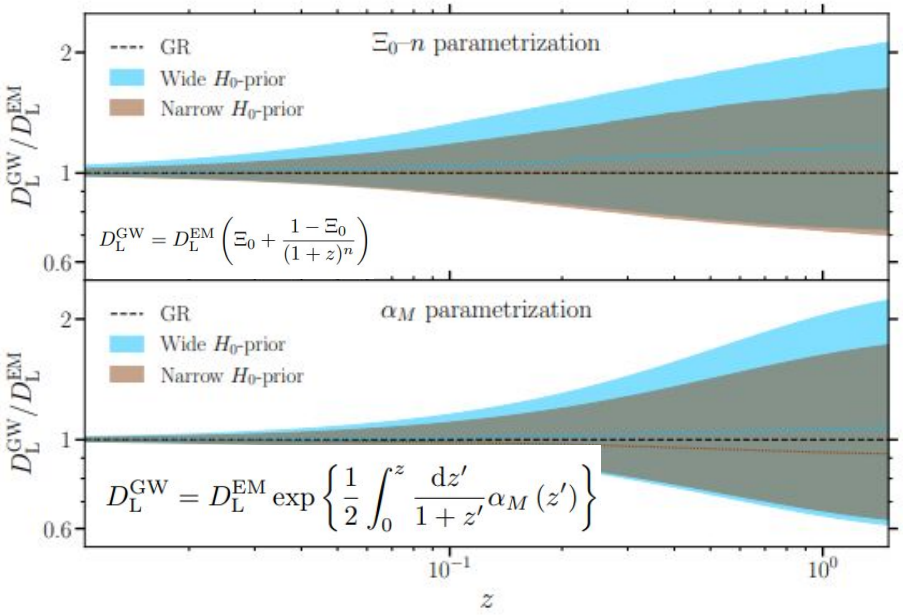

Figure 9. Reconstructed ratio D_L^{GW}/D_L^{EM} as a function of cosmological redshift z, for the two modified gravity parametrizations considered, Ξ_0–n and α_M. In both cases the contours show the 90% CI with median (dotted curve) reconstructed from the wide-H_0 prior (orange) and narrow-H_0 prior (blue) analyses with the FULLPOP-4.0 mass model. The black dashed curve represents the GR limit. Note that the reconstructed distance ratio is asymmetric at higher redshifts.

GRAVITATIONAL WAVE BACKGROUND

Cosmological GW background: signature of the Early Universe Inflation, preheating, reheating (10^{-18} – 10^{8} Hz); Phase transitions (a narrow band feature peaking at 10^{-12} Hz + broadband component in the band 10^{-5} – 1 Hz). Cosmic strings (10^{-10} – 10^{10} Hz); Alternative cosmologies

Astrophysical GW background: Such a GW background may result from the superposition of a large number of unresolved sources since the beginning of stellar activity. Its detection would constrain the physics of compact objects, the IMF, the star formation history. It would probe the Universe at z ~ 0.02–10. However, from the point of view of detecting the cosmological background produced in the primordial Universe, the astrophysical background is a 'noise', which could possibly mask the relic cosmological signal

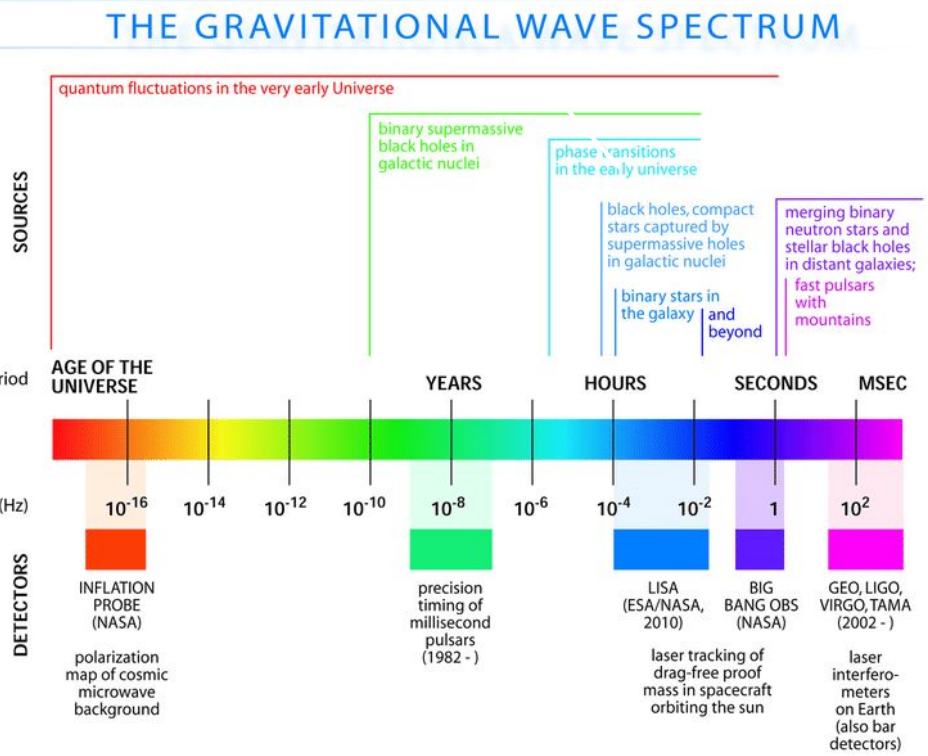

PULSAR TIMING ARRAY

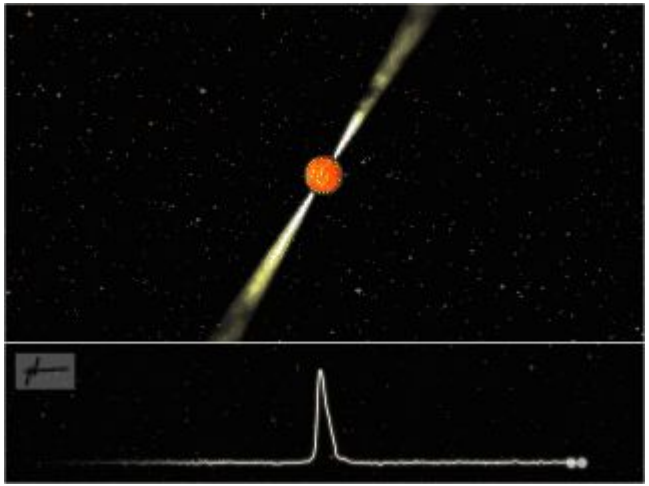

Highly magnetized rotating neutron stars, ultra-precise stellar clocks:

- **Beamed radio pulses emitted from magnetic poles**
- **Periods of 10^{-3}-1 s.**

Array of pulsars across the Milky Way can be used as GW detector of galactic dimensions:

- **Look for tiny distortions in pulse travel times caused by nanohertz GWs.**
- **Signal builds up over time; monitor PTA over years and decades.**

Which pulsars are suitable ?

Ordinary pulsars:
~ 3350 known objects;
NS_{age} < few 10^7 yr

relatively long pulses & rotational irregularities

Recycled pulsars:
~ 500 known objects;
NS_{age} > 10^8-10^9 yr

The most rapidly rotating are known as millisecond pulsars

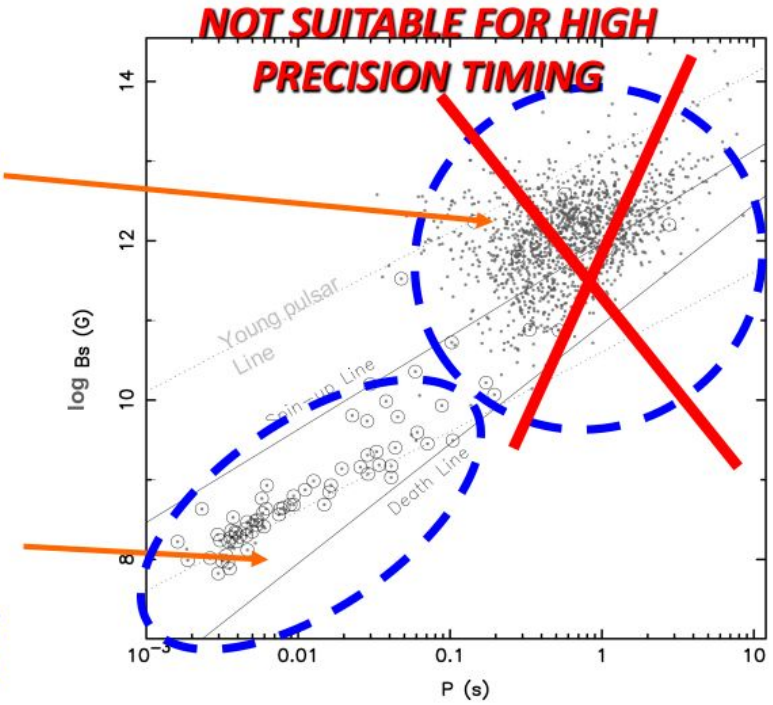

ATNF Pulsar Catalogue Feb 2024

Pulsar periods can sometimes be measured with unrivalled precision E.g. on Jan 16, 1999, PSR J0437-4715 had a period of:

5.757451831072007 ± 0.000000000000008 ms

PULSAR TIMING ARRAY

TIMING: Performing repeated observations of the Times of Arrival (ToAs) at the telescope of the pulsations from a given pulsar and searching the ToAs for systematic trends on many different timescales, from minutes to decades

The key quantities are the RESIDUALS:
i-th residual r_i is the difference in spin phase Φ between the observed phase of arrival of the i-th pulse and the phase of arrival of that pulse as predicted by the model:

$$r_i = \phi_{\mathrm{observed,i}} - \phi_{\mathrm{model,i}}$$

E.g.: Expected residual due to the passage of a GW emitted by a double SMBH
with a total mass of $5.4 \cdot 10^{10}$ M_{sun} and an orbital period of order ~yr (Jenet+2004)

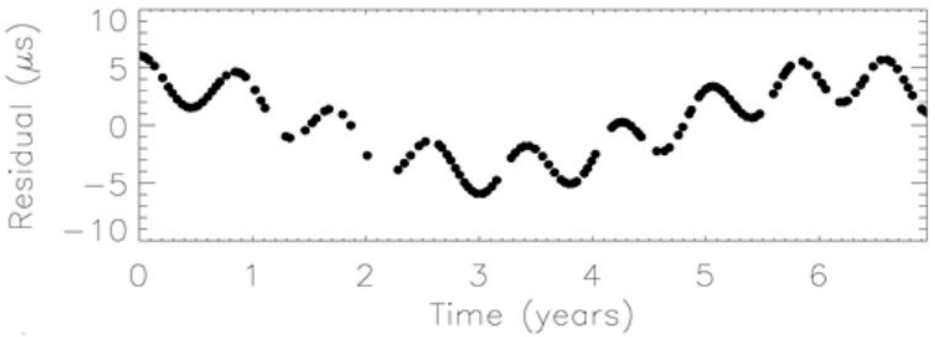

PULSAR TIMING ARRAY

Pulsar Timing Array: Using a number of pulsars distributed across the sky it is possible to separate the timing noise contribution from each pulsar from the signature of the GW background, which manifests as a local (at Earth) distortion in the times of arrival of the pulses which is common to the signal from all pulsars.

- **Clock errors**
  All pulsars have the same TOA variations: **Monopole** signature
- **Solar-System ephemeris errors**
  Dipole signature
- **Gravitational waves background**
  Quadrupole signature

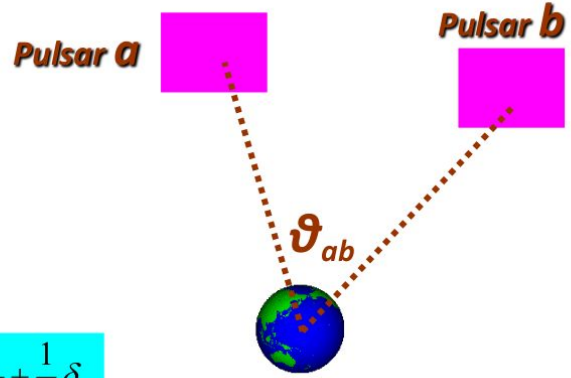

$$\zeta(\theta_{ab}) = \frac{3}{2}\left(\frac{1-\cos\vartheta_{ab}}{2}\right)\log\left(\frac{1-\cos\vartheta_{ab}}{2}\right) - \frac{1}{4}\left(\frac{1-\cos\vartheta_{ab}}{2}\right) + \frac{1}{2} + \frac{1}{2}\delta_{ab}$$

[slide adapted from Manchester 11]

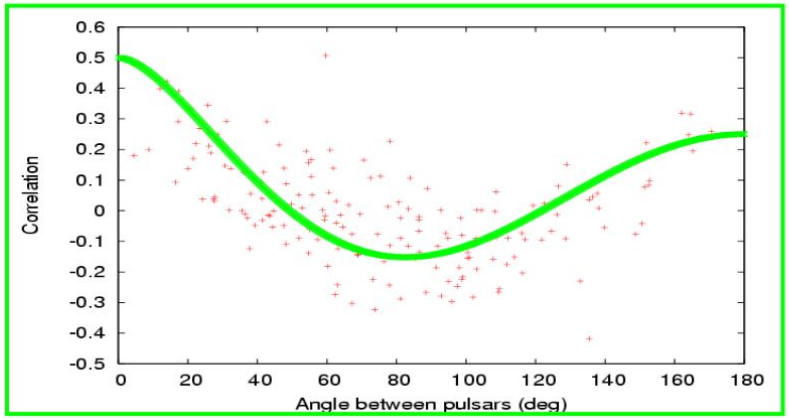

Hellings & Downs [1983]: correlation that an isotropic, stationary and stochastic GWB leaves on the timing residuals of pairs of pulsars a and b separated by angle ϑ_{ab} in sky

PULSAR TIMING ARRAY

PULSAR TIMING ARRAY

Evidence (2 - 4.6 σ) for quadrupole correlation signal from different collaborations.

The signal can be interpreted as:

1. **Cosmic population of in-spiralling SMBHB (realistic)**
2. **New Physics (speculative)**

2306.16213: NANOGrav

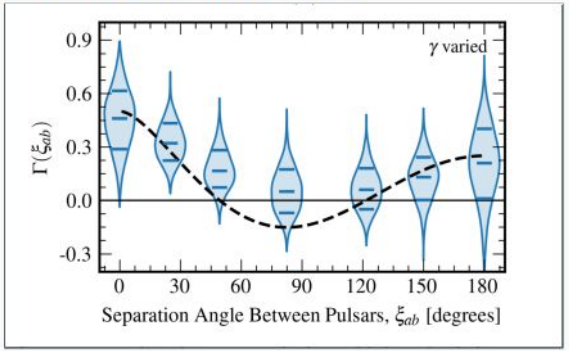

68 pulsars, 16 yr of data, HD at $\sim 3 \cdots 4\,\sigma$

2306.16214: EPTA+InPTA

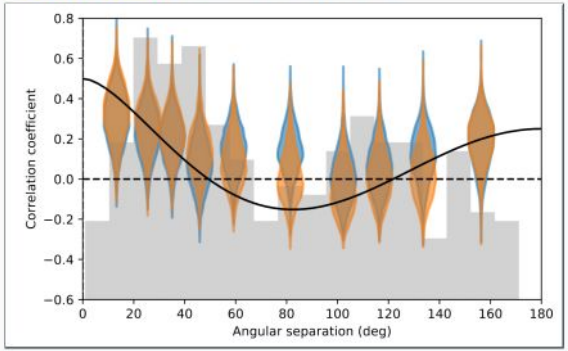

25 pulsars, 25 yr of data, HD at $\sim 3\,\sigma$

2306.16215: PPTA

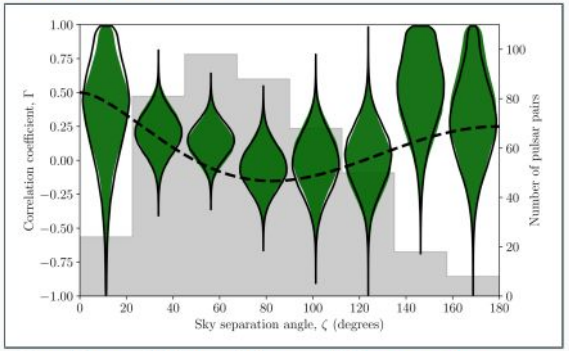

32 pulsars, 18 yr of data, HD at $\sim 2\,\sigma$

2306.16216: CPTA

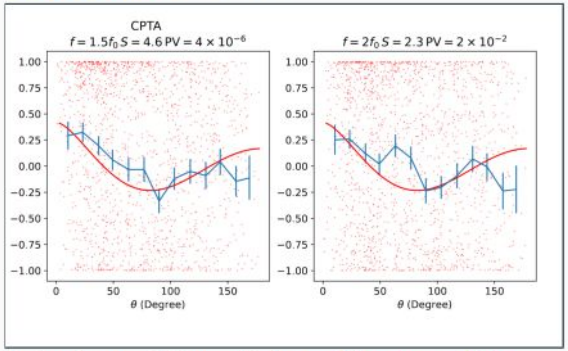

57 pulsars, 3.5 yr of data, HD at $\sim 4.6\,\sigma$

GW background due to Super Massive Black-Hole Binaries (SMBHBs):

Current paradigm is that [e.g. Ferrarese & Merrit 2000]:

- **mergers are an essential** part in galaxy formation and evolution
- **nuclei of most (all?)** large galaxies **host Massive BH(s)** i.e. mass $M \gtrsim 10^6\ M_\odot$

When reaching orbital separation *a* of less than about 1 pc, GW emission at frequency *f* become the dominant term in energy loss, making the MBH binary to shrink faster and faster

$$f \sim 3\ \mathrm{nHz} \left[\frac{M}{10^9 M_\odot}\right]^{1/2} \left[\frac{a}{0.01\ \mathrm{pc}}\right]^{-3/2}$$

PULSAR TIMING ARRAY

Expected Strain Spectrum of GWB:

In the simplest picture, the expected amplitude spectrum from the ensemble of these **MBH binaries** (supposed to be isotropic and stochastic) is [e.g. Phinney 2001; Jaffe & Backer 2003]:

$$h_c(f) \sim f^{-\alpha} \text{with} \quad \alpha = 2/3$$

with a "strain" amplitude h_c theoretically expected in a large range [e.g. Jaffe & Backer 2003, Rosado et al 2015, Sesana et al 2016, Kelly et al 2017, Zhu et al 2019]

$$h_c \approx 6 \cdot 10^{-17} \rightarrow 8 \cdot 10^{-15}$$

around frequency f_{GWB} = 1 yr^{-1}.

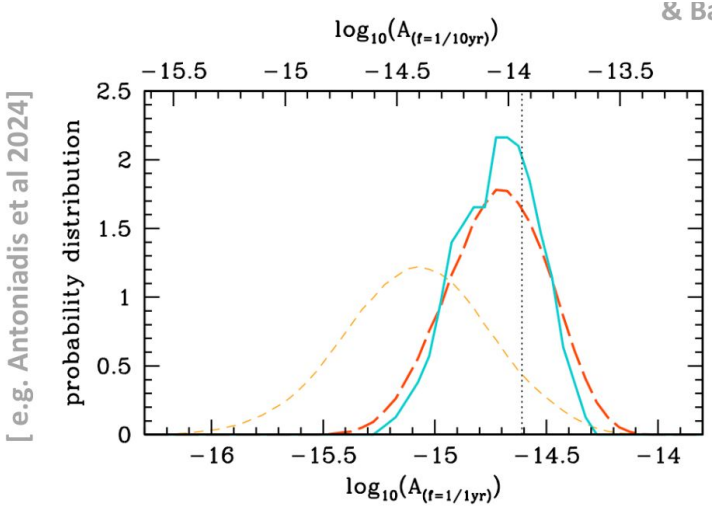

In terms of the time-domain power spectrum of the timing residuals this leads to

$$P(f) \propto \frac{h_c^2(f)}{f^3} = f^{-3} \cdot f^{-4/3} = f^{-13/3}$$

Observed Strain Spectrum of GWB:

2306.16213: NANOGrav

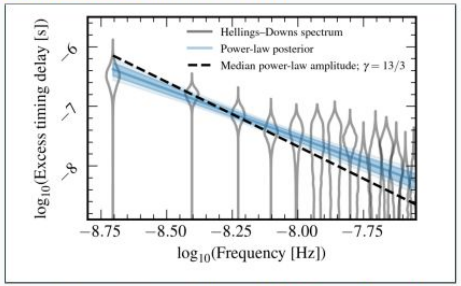

68 pulsars, 16 yr of data, HD at $\sim 3 \cdots 4\,\sigma$

2306.16214: EPTA+InPTA

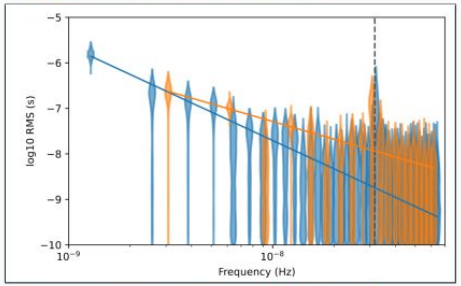

25 pulsars, 25 yr of data, HD at $\sim 3\,\sigma$

2306.16215: PPTA

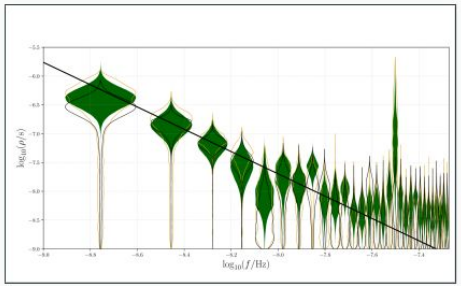

32 pulsars, 18 yr of data, HD at $\sim 2\,\sigma$

2306.16216: CPTA

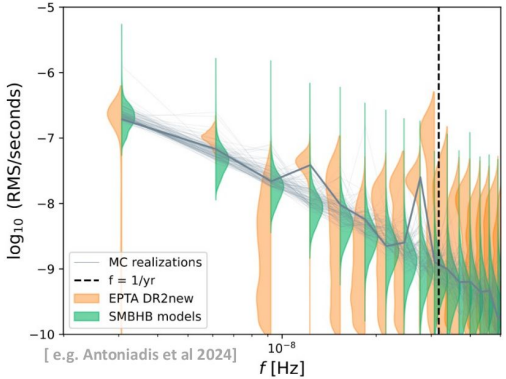

[e.g. Antoniadis et al 2024]

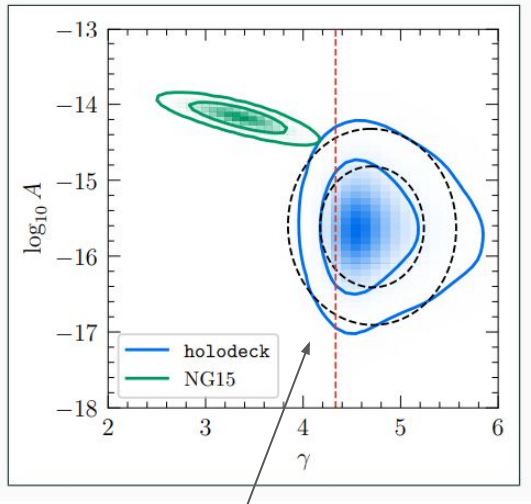

Simplest models of binary evolution (holodeck) struggle to explain the data (NG15), but many sources of systematic can hamper the interpretation of the results

Many Beyond-Standard-Model models predict GWB from the Big Bang:

Inflation

- Nonminimal blue-tilted models
- Interplay with CMB observables

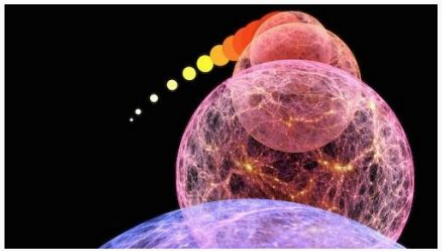

Phase transition

- Modified QCD transition, dark sector
- Complementary to laboratory searches

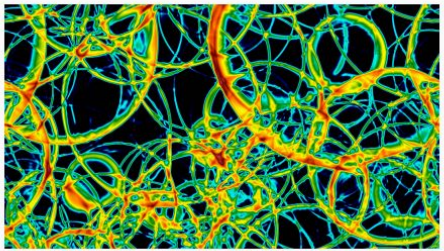

Cosmic defects

- Cosmic strings, domain walls
- Access to grand unified theories

Scalar perturbations

- Associated with primordial black holes
- PBH dark matter, supermassive BHs

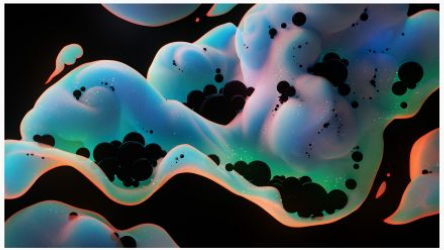

PULSAR TIMING ARRAY

The NANOGrav 15 yr Data Set: Targeted Searches for Supermassive Black Hole Binaries: Agarwal+25

First targeted searches for continuous gravitational waves (CWs) from 114 active galactic nuclei (AGN) that may host supermassive black hole binaries, using the NANOGrav 15 yr data set

IDEA: The source parameters (specifically sky location and frequency) are fixed by electromagnetic priors. Consequently, the relative amplitude and phase of the CW response in each pulsar are fully determined by the array geometry.